A Method to Characterize Gas Turbine Vane Thermal Performance Using Infrared Thermography

Shubham Chowdhuri

Thesis submitted to the Faculty of the
Virginia Polytechnic Institute and State University
in partial fulfillment of the requirements for the degree of

Master of Science
In
Mechanical Engineering

Srinath V. Ekkad, Chair
Wing F. Ng
Rui Qiao

February 5, 2018

Blacksburg, VA

Keywords: Gas turbine; infrared thermography; thermal performance; simplified technique

A Method to Characterize Gas Turbine Vane Thermal Performance Using Infrared Thermography

Shubham Chowdhuri

ABSTRACT

Gas turbine vanes find themselves in very hostile environments – extremely high temperature combustion gases, much exceeding material melting temperatures, flowing over them at enormous pressures. It is necessitated due to the increased efficiency and power output at these conditions. However, this also means that, in spite of the technological advancements made, these parts need frequent repairing compared to parts placed in milder environments. Primarily due to economic reasons, gas turbine parts are repaired by companies other than the original equipment manufacturer (OEM). While multitude of condition monitoring techniques have been developed and are used in the industry for regular maintenance checks, there is no easy way to characterize the impact on thermal performance of the repairing processes involved. This thesis reports the development of a technique to address this issue. It also chronicles the test rig design, experiments conducted, development and significance of the thermal performance metric. Heated air (250℃ – 300℃) is flown through the internal cooling passages of 8 samples each of OEM and repaired parts at two different pressure ratios (vane inlet over ambient pressure), 1.1 and 1.3. First, steady state mass flow rates through each airfoil (one part is a cluster of 4 airfoils) is experimentally determined and compared among the OEM and repaired sample sets. Second, a transient experiment is run and the surface temperatures of the airfoils are measured using multiple infrared cameras viewing both the pressure and suction side of the airfoils. A parameter involving localized vane surface temperature, airfoil inlet temperature and ambient temperature is formulated to characterize the vane thermal performance. Using statistical analysis, it is found that there is no significant difference between the OEM and repaired samples tested. The development of the discussed technique, it is expected, will help companies in the gas turbine vane repairing business to qualify their parts in a robust and efficient manner without the need to invest a

lot of money in buying precision equipment, or, control chambers. Finally, a couple of further studies are recommended to further improve the qualifying procedure and thereby increase the efficiency of the technique.

A Method to Characterize Gas Turbine Vane Thermal Performance Using Infrared Thermography

Shubham Chowdhuri

GENERAL AUDIENCE ABSTRACT

Most manufactured parts, during its lifetime, go through wear and tear of some form. Some much more than others – a gas turbine vane is one example, owing to the hostile environments it finds itself in. While repairing turbine vanes make economic sense instead of replacing the worn-out vanes with new ones, due care must be taken to ensure that the repairs pass high quality standards of the original manufactured parts. Most, if not all, companies in the turbine repairing business rely on room-temperature air-flow testing through the internal passages of these vanes to qualify their repaired parts. This is done partly due to the complexity in replicating engine-like conditions in a test environment in addition to being very time-intensive. While room-temperature air flow comparison between repaired and original parts is a necessary test, it does not paint the whole picture. Thermal performance, or, how the vane exchanges heat with the surrounding media, is the other part which completes the puzzle. A plurality of techniques has been developed to ascertain the thermal performance of gas turbine vanes, however, these are limited in the scope of their applicability – the reason why industry is still mostly relying on airflow measurements for their part qualification. In this study, a new technique has been proposed which is agnostic of the unavoidable variations in operating conditions and easy to apply while still upholding high quality standards. This translates to huge savings to organizations which are in the business of repairing original parts, not necessarily restricted to gas turbine industry.

ACKNOWLEDGEMENTS

Foremost, I would like to express my sincere gratitude to my advisor, Dr. Srinath Ekkad, for his motivation, encouragement, and, for believing in me at all times. Without your support and guidance this work would not have taken shape. I would also like to thank my advising committee members, Dr. Wing Ng and Dr. Rui Qiao for their valuable insight and guidance in this project. Dr. Ng, especially, instilled in me the importance of looking at the big picture – benefits of which I would intensely appreciate during my internship experience. And, I am confident, in my future work life as well.

This work would not have been possible without the support of the project sponsor, Trilotus Aerospace. Especially, I would like to thank Dr. Raj Thamburaj for his encouraging words even at times when things did not seem encouraging. Thank you for your unwavering support.

I would like to thank Dr. Jaideep Pandit and Dr. Prashant Singh for their crucial contributions throughout the project duration and beyond. Their experience and brilliance helped transform what would have been just-another-method into the present work. I also sincerely acknowledge the immensely helpful Mechanical Engineering staff – especially, Diana Israel.

Finally, I would like to thank my family for their love and support all throughout. All of this, everything, I owe to you.

TABLE OF CONTENTS

LIST OF FIGURES

LIST OF TABLES

CHAPTER 1

This chapter provides the necessary background for this work and motivates the research problem. A brief background 1.1 regarding gas turbine blade cooling requirement and condition monitoring is discussed first, followed by a literature review in section 1.2 highlighting the relevant works that dealt with characterizing the thermal performance of gas turbine blades specifically using infrared thermography techniques. Lastly, Section 1.3 contains the mapping for the remainder of the document.

1.1 Background

Thermal efficiency and power output of gas turbines, which are used for aircraft propulsion as well as for land-based power generation, increases with increasing turbine inlet temperatures. Thermal efficiency increase from 18% for the first gas turbine to 40-45% for modern gas turbines in simple cycle operation has been brought about, partly, due to the increase in turbine inlet temperatures from 900℃ to about 1500℃ (Powel 1991). These extreme temperatures far exceed the melting temperatures of the materials used for the construction of the hot gas path components. Besides, operating at such high temperatures also activates other modes of failure. In order to allow safe operations of hot gas path components, sophisticated internal and external cooling technologies are employed. Relatively colder air bled off from the compressor discharge is routed through internal cooling passages of turbine blades. Turbine internal cooling passages typically contain rib turbulators, plenum chamber for leading edge jet impingement and pin-fin arrays for trailing edge cooling. These heat transfer enhancement concepts are used to achieve higher rates of heat transfer between the coolant and the hot internal walls of turbine blades. As the coolant flows through the internal cooling circuits, part of coolant also escapes through the film cooling holes to create a cool protective layer on the outer surface of turbine blades.

The turbine inlet temperatures can be pushed to higher and higher levels by increasing the amount of air flow through the internal passages to carry away more heat, however, there

is an associated counteractive impact: increased pressure drop and reduction in engine performance. Thus, the design of modern gas turbine involves innovative methods based on iterations of techniques discussed in the preceding paragraph. Figure 1 shows the cooling arrangements on a typical modern gas turbine blade. A comprehensive review of the different techniques developed and used in the industry can be found in (J.-C. Han, Dutta, and Ekkad 2012). The best design would try to minimize the amount of compressor bleed air to cool the blades by increasing the heat extraction efficiency and thus, maximize the benefits of high turbine inlet gas temperature.

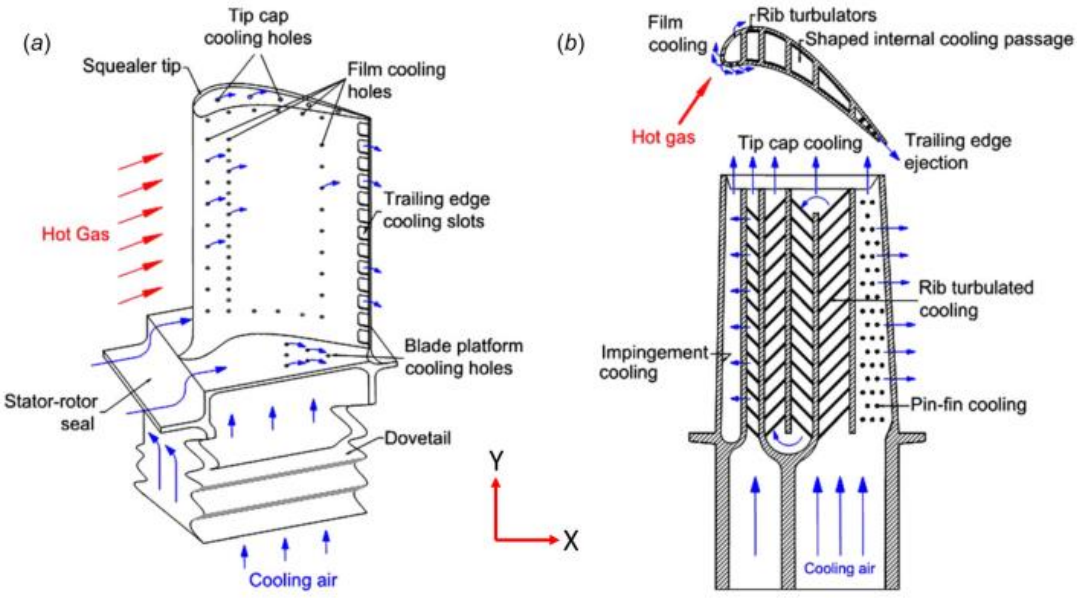

Figure 1: Gas turbine blade cooling techniques (a) external cooling; (b) internal cooling (J. C. Han and Rallabandi 2010)

As a direct consequence of exposure to high temperatures, turbine blades and vanes experience mechanical damage through either creep or thermal fatigue (low cycle fatigue) and high temperature corrosion. Use of light alloys, such as that of Aluminum or steel, is not feasible for turbine parts since they cannot generally be designed to provide acceptable creep properties at the high temperatures needed for efficient turbine operation. The most common materials for turbine blade manufacture are nickel-based “super-alloys” because they retain strength over a wide temperature range and hence are less susceptible to creep failure. Besides, they also form a thick, stable, passivating oxide layer, when heated, thus

protecting the surface from further damage. Report about common failures in gas turbine blades can be found in (Carter 2005)

Even though gas turbine parts are designed to the highest engineering standards, due to the extreme environments prevailing in the regions these components operate at, gas turbine vanes and blades need regular maintenance and, on average, go through a few repair cycles during in service-life. Gas turbine vanes, in particular, may distort due to thermal gradients; form cracks on the vane surface; undergo metallurgical degradation during engine operation; among other failures. Due to the high replacement costs of these parts, economically, it is prudent to repair them by having a robust maintenance procedure in place to catch defects early instead of replacing these parts. Different parts of the gas turbine blades and vanes encounter different failures and are, consequently, subjected to different restoration procedures. A few examples are shown in Figure 2. Moreover, special type of coatings—known as thermal barrier coating (TBC)—are applied, both on internal and external surfaces, to add a further layer of protection against oxidation and heat. Account of various gas turbine blade and vane repair techniques can be found in (Antony and Goward 1988; Carter 2005; Mazur et al. 2005).

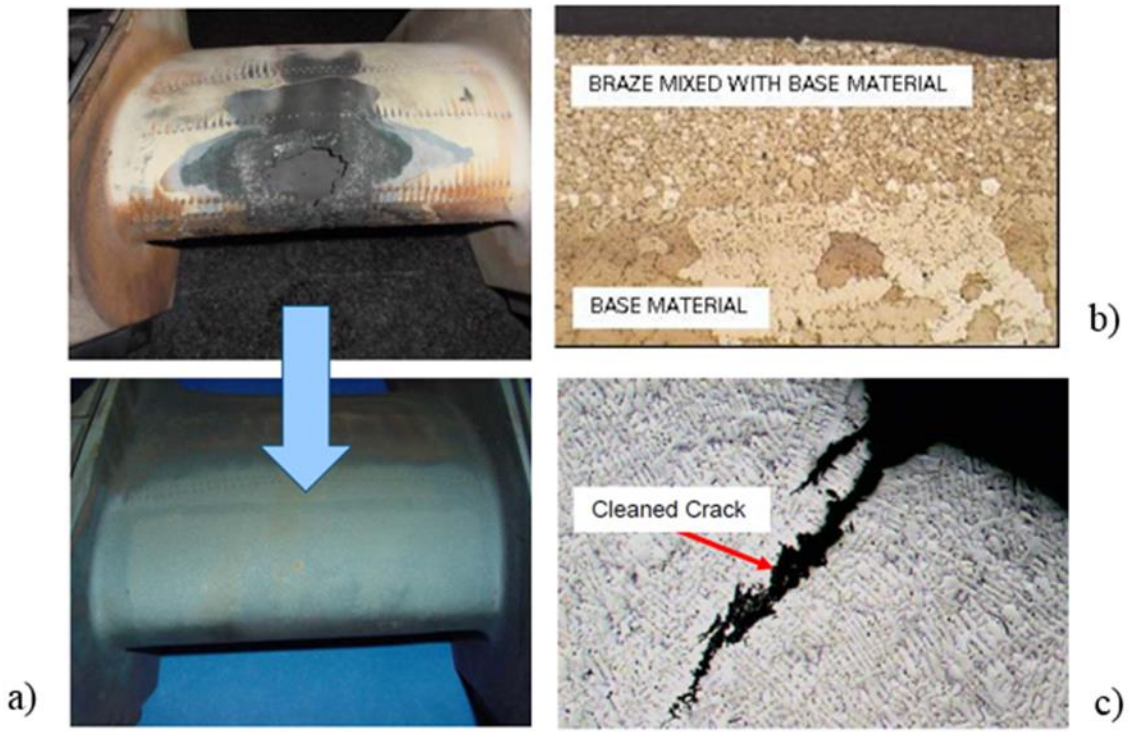

Figure 2: a) Turbine Vane Leading Edge Coupon Repair, b) Overlay Brazed Nickel-Based Alloy, c) Cleaned Crack in Cobalt-Based Alloy (McGraw et al. 2006)

Early detection and localization of defects and deviations from in gas turbine components, especially, turbine vanes and blades is key for safety. In this regard, a plurality of techniques and methodologies have been developed and proposed to inspect gas turbine blades and vanes utilizing coordinate measuring machines (CMMs), acoustic sensing, eddy current probes, infrared thermography, X-Ray diffraction (XRD), scanning electron microscopy (SEM), among others. (Harrold and Sanjana 2002; Park et al. 2002; Urich and Freeman 1979; Vardar and Ekerim 2007; Woodmansee 2002; Zorner 1995). Of these, infrared thermography based techniques has benefited from continued interest and support from industry as well as the research community. This has resulted in the availability of infrared cameras with a wide variety of resolutions and thermal sensitivities and at nearly every price range. One reason for its adoption is that IR thermography is fast—this advantage is exploited in a particular form of transient pulsed thermography based monitoring. Second, unlike point measuring devices, like thermocouples, relatively large areas can be inspected quickly using IR. In addition, infrared thermography based techniques do not require any instrument or device to be in contact with the component being inspected. Moreover, it has none of the harmful effects of radiation associated with technologies such as X-Ray imaging. Such benefits has led to the development of different techniques utilizing IR thermography in the Non Destructive Testing (NDT) community, few of which are Dynamic Thermal Tomography (Swiderski 2009), Pulsed-Phase and Lock-In Thermography (Maldague, Galmiche, and Ziadi 2002; Meola et al. 2006), Thermographic Signal Reconstruction(Shepard 2003)

One other method to carry out Non Destructive testing is by using liquid crystal thermography. It is a commonly used technique in gas turbine cooling research. Some of the early developments on liquid crystal were reported by (Ireland, Wang, and Jones 1993). Liquid crystals when subjected to either heated or cold air change colors in a particular temperature band, and is often used in calculation of heat transfer coefficient for internal and external flows and film cooling effectiveness for external flows. The details of application of liquid crystal are documented by (Ekkad and Han 2000). More recently, due

to advancements in data acquisition, liquid crystal color change video quality, frame rates; the liquid crystal thermography technique has further advanced. Studies carried out at Advanced Propulsion and Power Laboratory at Virginia Tech has successfully demonstrated the implementation of liquid crystal thermography for stationary and rotating internal flows experiments, where the authors viewed at the liquid crystal color change through an optically clear material (Ravi, Singh, and Ekkad 2017; Singh, Ji, et al. 2017; Singh, Li, et al. 2017a, 2017b, Singh and Ekkad 2016, 2017a, 2017b, 2017c; Singh, Ji, and Ekkad 2018; Singh, Pandit, and Ekkad 2017; Singh, Ravi, and Ekkad 2016). One limitation of using TLC for non-destructive testing of engine hardware is that TLCs are commercially available from 0C to about 60C, and their accuracy decreases at higher temperatures.

Although the development of various condition monitoring techniques has resulted in reduced component downtime, improved reliability and safety, and cost savings; much can be gained from thermal performance characterization at the time of regular condition monitoring. More importantly, thermal performance comparisons, with original parts (OEM), become utmost important after components have been repaired or replaced. Gas turbine components are regularly repaired by companies other than the OEMs primarily because of economic reasons. These companies frequently use processes which differ from the OEMs. In some cases, there might be additional processes involved, for example, the company may choose to use a TBC of different thickness and/or material—usually done to improve the longevity of the components. However, the impact of these variations, mainly geometrical, needs to be assessed prior to installation. Clearly, condition monitoring techniques are not applicable at this stage as they cannot provide information on the thermal performance impact of these changes.

1.2 Related Work

For repaired parts, it is common practice to inspect the part, a portion of the part or assembly of the parts, by flowing air (mostly at ambient temperature) or water through the cooling circuit—otherwise known as the “flow check” method. The flow obtained, as a function of pressure ratio, is then compared to historical data of properly functioning

repaired parts, or similar flow check data available for OEM parts. Acceptance of the part is based upon the flow falling within the upper and lower specification limits. This technique is relatively simple and fast and provides valuable information on the flow capacities of the repaired parts. However, only flow inspection does not guarantee similar heat transfer characteristics. Due to the variability in manufacturing these components, there can be parts which pass the flow check but do not perform adequately thermally. This can lead to problems directly affecting the component, or, worse, in components downstream in the flow-path making root-cause failure analysis to trace back to the component far more complicated and cost intensive. As such, it becomes imperative to ascertain thermal performance of the components in addition to flow check as well, especially for parts in the hot gas path.

An innovative nondestructive and non-intrusive technique to measure full-surface internal heat transfer coefficients of turbine airfoils was proposed by Nirmalan et al. (Bunker and Nirmalan 2011; Nirmalan, Bunker, and Hedlung 2003). In this technique, the authors utilized transient infrared imaging of a cooled or heated airfoil, in conjunction with flow rate and geometry measurements, to generate 2-D map of internal heat transfer coefficients of the airfoil. Although the method produces detailed information of heat transfer coefficients, similar to information obtained using liquid crystals (Ekkad and Han 2000) for internal surfaces, it requires detailed information about the geometry of the part. Further, it uses the geometry information, flow data and external surface temperature data to iteratively solve a 3D inverse transient conduction problem to predict the correct heat transfer coefficient values. With the availability of today's computing power, the impact on computing time might be minimal, however, for a manufacturing industry setting where thousands, maybe millions, or parts are produced, even a small saving in per unit time/energy can lead to tremendous gains overall.

In this regard, one of the earlier efforts to compare thermal performance of gas turbine parts using infrared thermography by Bantel and Mack (Bantel and Mack 1987), were quite economical. Their technique, utilizing transient infrared imaging, involved passing heated air through the internal cooling passages of the airfoil and measuring and comparing the transient response with a reference. In another variation (Bantel 1992),

heated air is first forced into the hollow interior during the heat-up cycle, after which the system is allowed to stabilize for a predetermined time, followed by a cool-down cycle where cold air is passed. An infrared camera captures the transient response during both the heat-up and cool-down cycles. Selected parameters, derived from the transient response, are then used to compare the part against a statistical base reference derived from the inspection of other similar parts, as in (Bantel and Mack 1987). A slightly modified technique, extended by the use of concept from to lock-in thermography, has been described by Beckeiz et al. (Beckeiz, Sperling, and Carl 1998) and Stiglich et al. (Stiglich et al. 1998). Here, too, they compare the thermal response to a "known standard". In yet another variation of (Bantel and Mack 1987) developed by Bunker et al. (Bunker and Allen 2010), first and/or second derivatives of the temperature maps, captured using transient infrared thermography, are computed and compared to baseline values to determine if the part meets desired specifications.

While the techniques developed in (Bantel 1992; Bantel and Mack 1987; Beckeiz, Sperling, and Carl 1998; Bunker and Allen 2010; Stiglich et al. 1998) provide useful information about the thermal performance of the tested parts, to get useful results the experimental conditions need to tightly controlled. For example, the temperature to which the fluid is heated in the heat-up cycle for all the tested parts needs to be in a small tolerance band of few degrees if meaningful comparison is sought. For small number of parts to be tested, this might not pose a problem. However, in cases where large number of components need testing which might or might not be in the same physical location, tighter tolerances, more precise and expensive instrumentation, GR&R studies if multiple operators are used, might be necessitated. This study extends the methods developed and discussed in (Bantel and Mack 1987; Bunker and Allen 2010) and proposes a normalizing parameter that negates the impact of small variations in test and ambient conditions. This is expected to produce better quality data and minimize errors owing to variations in test conditions resulting in reduction, or, in the best case, elimination of false negatives.

1.3 Organization

This thesis has four chapters excluding chapter 1. Chapter 2 discusses the details of the samples that were tested—how the repaired parts differ from OEM, the internal cooling arrangement of these parts. It also goes over the design of the experimental test rig that was built for the development of the current technique including the formal test procedure followed. In addition, the procedure to calculate mass flow rate through an orifice plate and the infrared camera calibration technique are also discussed in this chapter. Next, a detailed comparison of airflow between OEM and repaired parts is made in Chapter 3. Following which, in Chapter 4, a technique is first described that characterizes the vane thermal performance using surface temperature data recorded through an infrared camera. This technique is then applied to make comparison between the same samples of OEM and repaired parts. Finally, concluding remarks along with directions for future research are presented in Chapter 5.

CHAPTER 2

2.1 Hardware description

To develop the methodology, baseline results had to be collected first from a selection of OEM parts to account for the variability in manufacturing processes. A total of 32 airfoils, 8 vanes of 4 airfoil sections each, were tested to form what will be termed as "upper" and "lower limits". Although, 32 airfoils do not capture the population variation of thousands of OEM parts, sufficient insight can be expected to be drawn from the test results of 32 airfoils at a reasonable confidence level. Based on similar logic, 32 airfoils, again 8 vanes of 4 airfoil sections each, of repaired parts were tested to draw conclusions from the study conducted to be discussed later.

The OEM and repaired parts tested in this study for the development of the technique were all a cluster of 4 airfoils each as mentioned above. Beside this geometrical similarity, the OEM and repaired parts differed greatly. While the OEM part was a single

cast piece, only the outer platform of the original OEM part was preserved in the repaired part. The rest, comprising 4 cast airfoil sections and inner platform were reverse engineered from the OEM part. This is shown in Figure 3. Further, the base material and external coating in the repaired parts were also reverse engineered. The internal coating, however, was unique to the repaired part and was not present in the original part design.

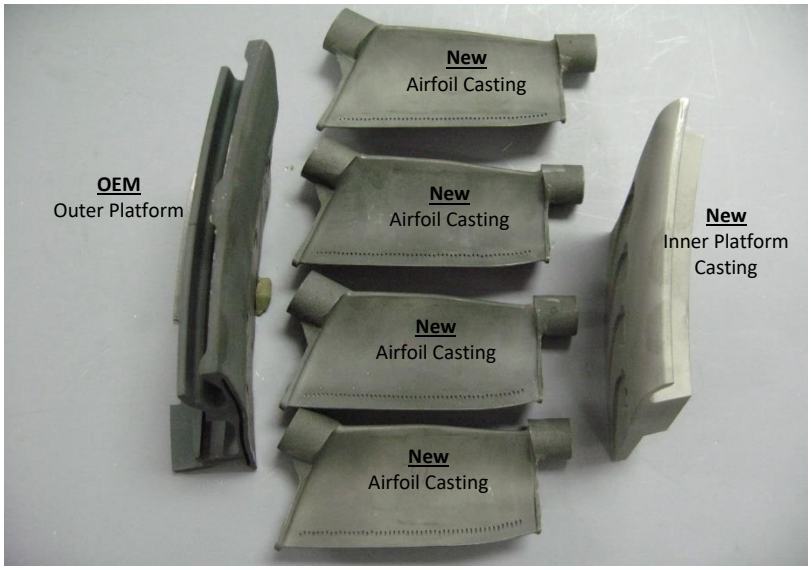

Figure 3: Representative repaired vane

Figure 4 shows the airfoil cluster representative of both the repaired and OEM parts. Cooling air ducted from a compressor stage upstream enters the airfoils through the outer platform ports. Thereafter, air travels through the vane to exit from the inner platform ports to provide cooling for components downstream in the flow path, for example, disks.

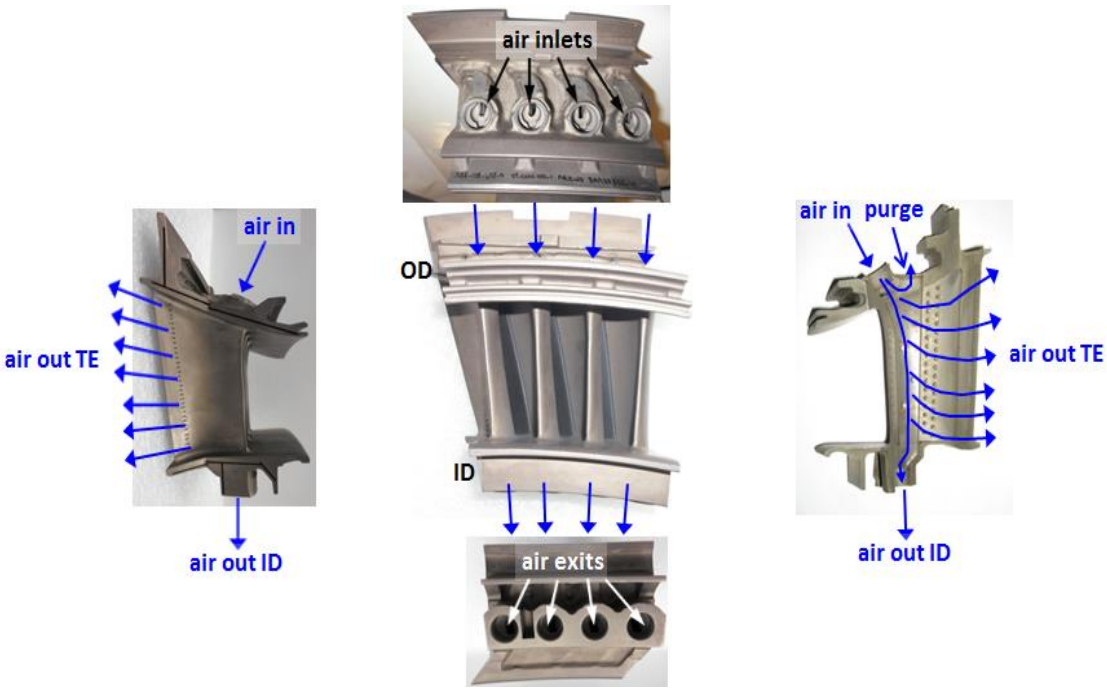

Figure 4: Vane showing cooling air flow circuits

Majority of the air entering the airfoil through the OD leaves through the ID cooling the airfoil mid-section. A portion leaves the airfoil through the trailing edge (TE) holes, while another small portion leaves through the purge hole. For the experiments carried out for this study, the purge holes were completely blocked in all cases and air was allowed to exit only through the inner port holes and TE holes – this has been termed as the Total flow circuit.

A holistic investigation was undertaken by the company which sponsored this research project to uncover geometrical variations, both internal and external, using techniques such as white-light scan, computed tomography x-ray, VMM and CMM scan. This evaluation uncovered that while there were differences in geometry between the repaired vane and the OEM vane which reduce the cooling air flow, these differences were in fact balanced by other differences which increased the cooling air flow. That is why, overall, in spite of the various differences observed between the two sets, the cooling air flow at room temperature was found to be quite similar between the repaired and OEM parts. However, due to various differences in the OEM and repaired parts introduced due

to manufacturing variations, the impact of high-temperature on internal air flow as well the thermal performance was unquantified.

Therefore, an attempt has been made in this study to first, quantify and compare the air flow rates through both sets of OEM and repaired parts. Following which, a technique that captures the variation in internal heat transfer capacity of the vanes, if any, using infrared thermography of the external surface, has been formulated and applied to the two sets of vanes.

2.2 Experimental Setup

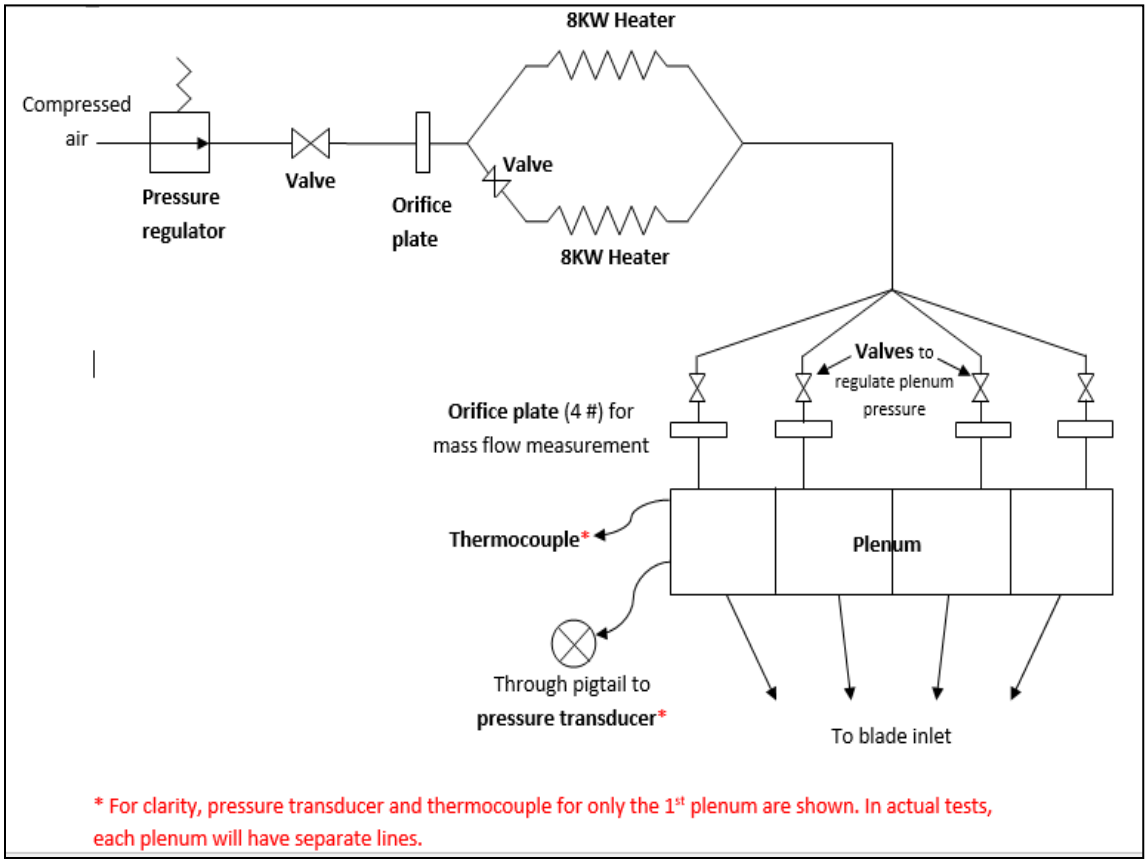

Figure 5: Schematic of the test setup

In the designed test rig, air discharged from the main compressor, installed at the Advanced Propulsion and Power Lab at VT, at 298 K and 80 PSI enters the combined

pressure regulator and filter (Rapidair K93218 NPT Filter Regulator). The pressure ratio at the vane inlet was set at a ballpark range using this regulator. The air then split into two separate lines to enter the two air heaters (Osram Sylvania SureHeat® JET, Part number F074719). These heaters were controlled using individual high-speed digital temperature controllers and solid state relay packaged together in the proprietary Osram Sylvania control system (SureHeat® JET Control Panel). Downstream of the heaters, the two lines merged into one before again splitting into 4 separate lines, each for one airfoil of the 4-vane cluster. The logic behind merging the separate lines from each heater before splitting them again was to homogenize the air so that variations in the heating capacity of the heaters were negated even though, specification-wise, both heaters dumped same amount of heat into the air. Besides, replacing one of the heaters with a higher or lower powered substitute, in case such a requirement surfaced, would not necessitate re-building the rig since the air streams were now mixed before the final 4-way split. After the 4-way split, one ball-valve for each line was placed – these were used for fine-tuning and accurate setting of the PR at the airfoil inlet. Air would then enter a section of straight pipe of length around 20 pipe diameters before encountering the orifice plates (Oripac Model 5300 from Lambda Square). These orifice plates were used to measure the mass flow rates through the individual lines. After another straight section of pipes around 8 pipe diameters, the pipes connected to flexible metal tubes which then finally connected to the airfoil inlet tubes using compression fitting. A high temperature sealant (X-Pando Pipe Joint Compound) was used to seal all threaded joints in the setup to arrest any leaks, if present. In addition, as the heated air moves through the lines, some of the heat is lost to the ambient due to various losses. To minimize these losses, insulation was wrapped around the pipes and fittings starting from the heaters till the inlet of the brazed tubes connected to the airfoils. A line diagram of the setup is shown in Figure 5 and a picture of the actual test setup is shown in Figure 6.

As has been mentioned earlier, the present technique was aimed at absorbing variations in operating conditions—like, ambient temperature, coolant inlet temperature—in its formulation. However, for the first part of the study where air flow rates are compared between OEM and repaired parts, in order to make legitimate comparisons and capture flow differences accurately, it was imperative that we maintain repeatable test conditions

in all cases. One parameter that dictates the air flow rate and, consequently, that was maintained across the set of experiments performed was the pressure ratio (PR): defined as the ratio of the pressure at the airfoil inlet to the ambient pressure.

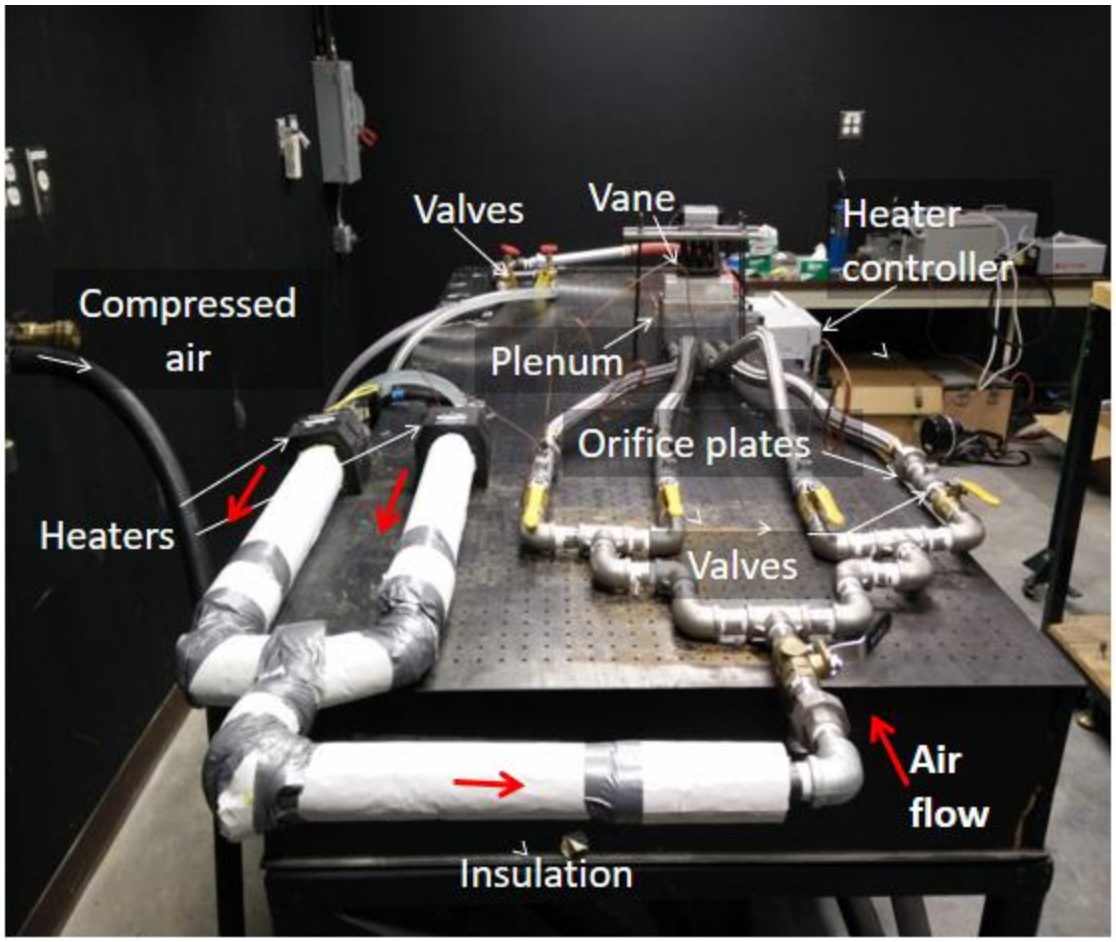

Figure 6: Picture of the actual test setup sans instrumentation and complete insulation

As such, the tests required monitoring airfoil inlet pressure. The temperature at the inlet was also monitored using a K-type thermocouple. The use of monitoring this temperature will be explained later in this document. Multiple plenum chambers, one for each airfoil, that supplies air and also has ports for pressure and temperature measurement was designed and manufactured, as depicted in Figure 7. However, establishing a leak proof mating between the airfoil inlet and plenum proved to be extremely difficult using the arrangement that needed to be tested. Specifically, as can be seen in Figure 3, the airfoil ID and OD port areas are curved and are at an angle to each other. Moreover, designing a

fixture to press the vane onto the plenum would have created disturbances to air flow through the ID. This would have resulted in re-distribution of airflow between ID and TE holes which was undesired. More robust methods of attaining leak proof mating though available, those options were either time or cost prohibitive or both. It was, therefore, decided to braze stainless steel tubes at the airfoil inlet which would then connect to the individual supply lines using compression fittings as is shown in Figure 8. Arrangements for pressure and temperature measurements were made in this case as well using a 4-way compression fitting.

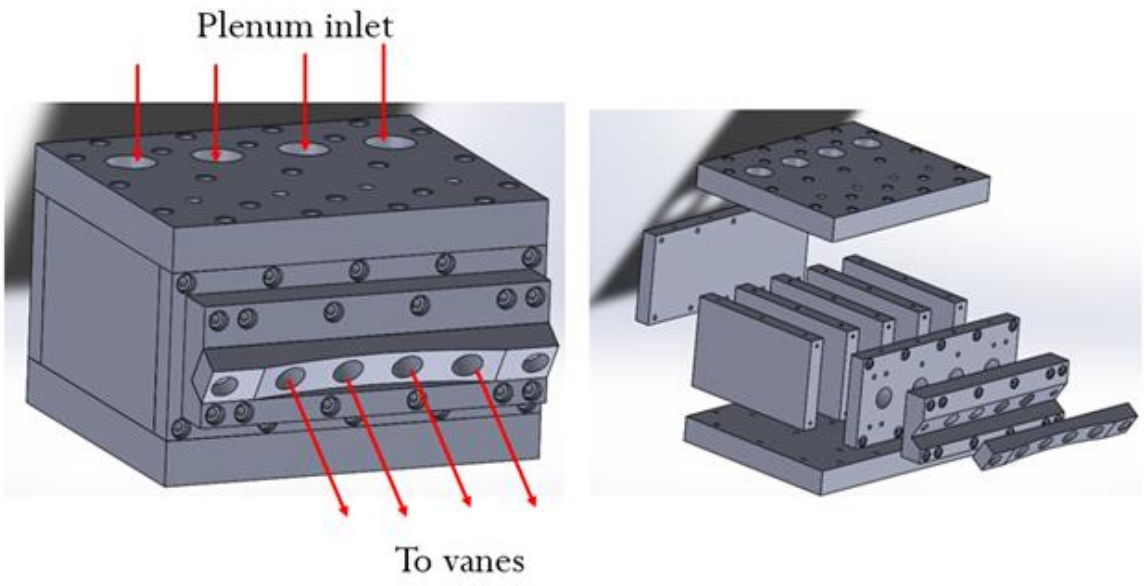

Figure 7: Original design for plenum

Besides pressure and thermocouple measurements, the designed setup also included 3 infrared cameras—FLIR SC6700, FLIR SC325, and FLIR A35—for monitoring airfoil surface temperatures. These cameras were strategically placed around the vane so as to cover the maximum possible surface area of the vane, as depicted in Figure 9. The actual arrangement of the cameras around the vane was as shown in Figure 10.

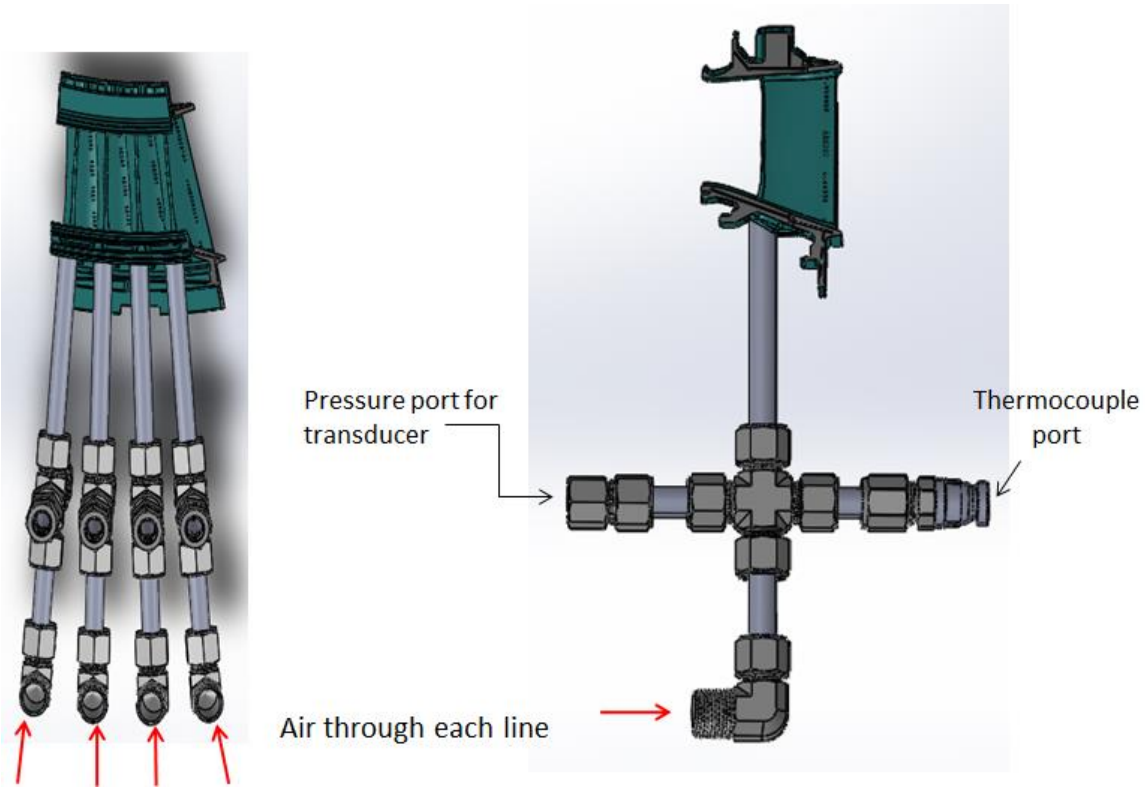

Figure 8: Brazed stainless steel tubes at airfoil inlet connected to supply lines using compression fittings

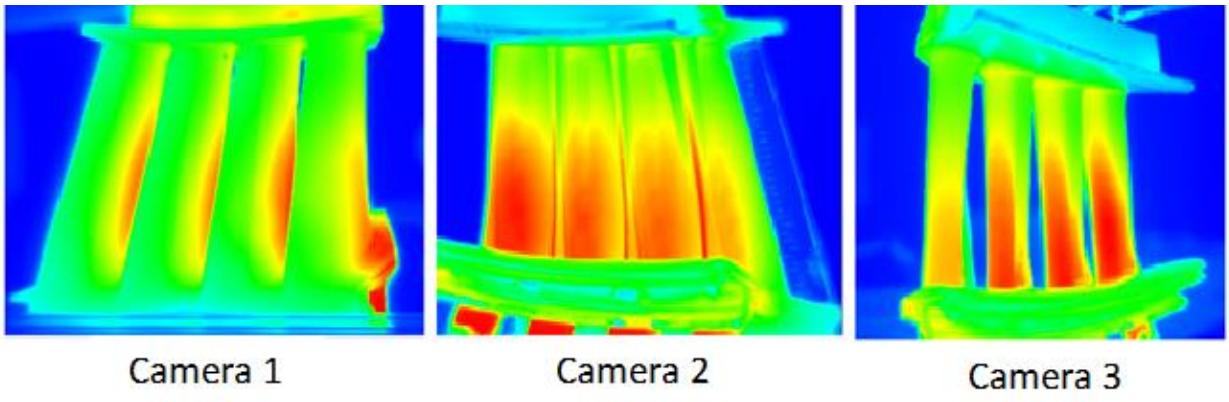

Figure 9: Infrared images as viewed by the three different cameras

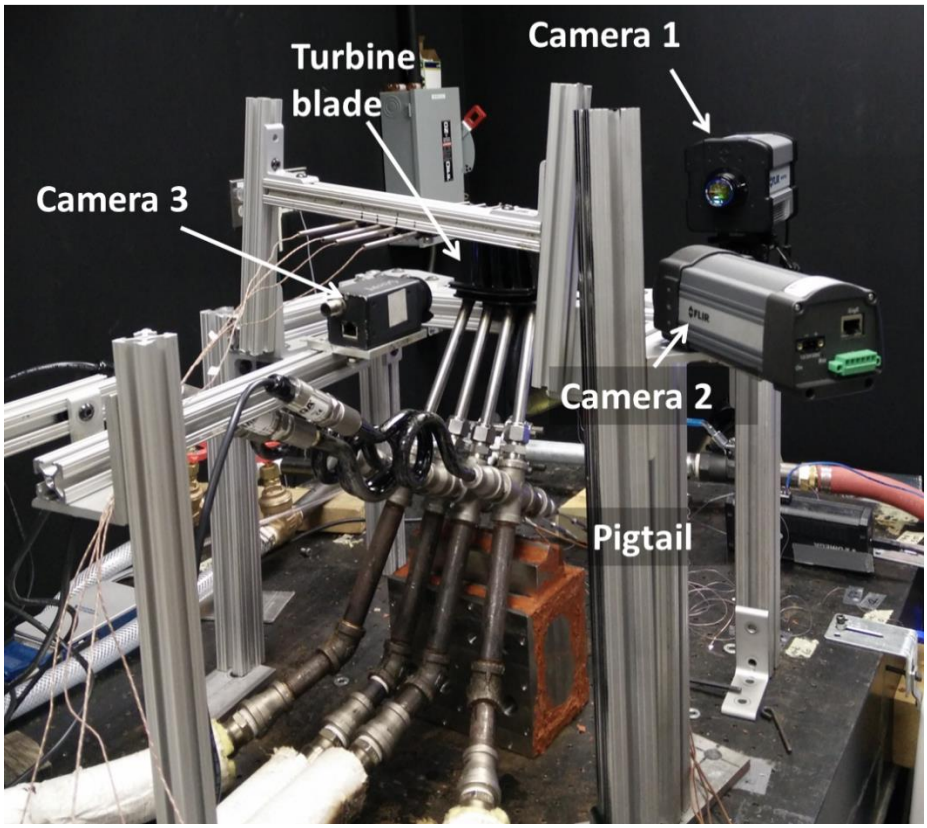

Figure 10: Final setup showing placement of IR cameras around the vane

2.3 Mass flow measurement using orifice plate

An orifice plate is a thin plate with a hole in it which, basically, creates an obstruction to the flow much like an hour glass does. Because of this, the velocity of the flow increases after the obstruction and consequently the pressure decreases by Bernoulli's principle considering an incompressible flow. This drop in pressure, in turn, can be related to the mass flow rate through the orifice.

Mass flow rate through an orifice plate can be estimated using the formula:

$$q_m = \frac{C_d}{\sqrt{(1-\beta^4)}} \epsilon \frac{\pi}{4} d^2 \sqrt{2\rho(p_1 - p_2)} \quad (1)$$

where: q_m = mass flow rate, kg/s

C_d = coefficient of discharge, dimensionless

β = ratio of orifice diameter, d to pipe diameter, D, dimensionless

d = internal orifice diameter, m

ε = expansibility factor, dimensionless

P_1 = pressure at the upstream tapping, Pa

P_2 = pressure at the downstream tapping, Pa

ρ = fluid density at the upstream tapping, kg/m^3

The coefficient of discharge (C_d) depends on many factors including the ratio of orifice diameter to pipe diameter (β), the type of pressure tappings (corner taps for the model used), and flow Reynolds number. Based on Reader-Harris/Gallager equation (ISO 2003), C_d can be calculated as:

$$C_d = 0.5961 + 0.0261\beta^2 - 0.216\beta^8 + 0.000521\left(\frac{10^6\beta}{Re_D}\right)^{0.7} + (0.0188 + 0.0063A)\beta^{3.5}\left(\frac{10^6}{Re_D}\right)^{0.3} + 0.011(0.75 - \beta)\left(2.8 - \frac{D}{0.0254}\right) \quad (2)$$

Since the calculation of Cd is dependent on the flow Reynolds number which is a function of flow velocity and thus flow rate, an iterative calculation procedure is employed in MATLAB to converge to the correct value for mass flow rate starting from a guess value of C_d.

The expansibility factor, ε, on the other hand is taken to be 1 because none of the test conditions exceed the limit $p_2/p_1 > 0.75$ for which the condition holds (ISO 2003).

Though orifice plates are rather inexpensive and provide an accurate way of measuring mass flow rates, they are limited by the range of their measurement capacity with a turndown of around 4:1. As such, orifice plates must be properly sized for the required test conditions for better accuracy. Furthermore, orifice plates only work well when supplied with a fully developed flow regime—the reason for having 20 pipe diameter straight sections upstream of the orifice in our setup. Another important parameter involved in the computation of the mass flow rate is the fluid density (ρ). Since our experiments involve air flow at high temperature, thermocouples are placed in the 4 individual sections

upstream of the orifice plates to capture the variations in density due to changing temperature.

2.4 Test procedure

The step-by-step outline of the operations performed in conducting a typical experiment is detailed below:

1. The airfoil pressure ratio is set coarsely using the main regulator and then fine-tuned using the valves to the desired set condition for the run.
2. Once the pressure is set, both the heaters are powered on and heated air is allowed to pass through the vane section finally leaving through the ID ports.
3. The temperatures at the airfoil inlets are allowed to reach steady temperatures.
4. During the heating period of the test rig, pressures at the airfoil inlet increase with time and deviate from the set PR condition—this is coupled with the variation in density due to changes in temperature. At this stage, the PR is set, for the final time, to the test condition using the valves upstream of the orifice plates.
5. At this steady condition, the air flow data is stored and IR cameras are initialized.
6. Both heaters are powered off simultaneously and cameras start recording surface temperatures.
7. Data is logged for a fixed time in all cases—40 minutes for PR 1.1 and 30 minutes for PR 1.3.
8. Air is allowed to pass through the vane till it reaches ambient temperature. At this point, the vane is replaced, and the test is repeated for the next vane.

One important observation to note here is that infrared thermography data was logged after the heaters were powered off, that is, during the cooling period. The reason behind this stems from the difficulty in maintaining pressures at the airfoil inlet at a steady value in the heat up period, mentioned in step 4 above. If data were logged during the heat up period, firstly, the time required for every run to complete would be close to an hour—a prohibitively high number. This would not only inflate the experimental time requirements but also the time required to process extremely large data sets captured by

the multiple infrared cameras. Moreover, logging data in the cooling period was more robust compared to recording heating period data in terms of repeatability. And, because we were able to consistently set the inlet pressure ratio for all experimental runs using the described procedure, a valid and consistent starting condition was attained for air flow rate and subsequent thermal performance comparison.

2.5 Infrared Camera Calibration

Prior to calibrating infrared cameras and taking any measurements, the vane surfaces were painted black (using Black Backing Paint available from thermometersite.com). This was done to improve the emissivity of the vane surface as the original parts had a metallic finish which are known to have poor emissivity values. Having a high emissivity test surface improved the fidelity of the test data. The infrared images were calibrated against thermocouples attached to the vane surface prior to the beginning of the experiments. Multiple thermocouples, at least 2 for each airfoil in the field of view of the infrared camera, were used for surface temperature measurements. Having multiple thermocouples helped in mapping different infrared camera output to actual thermocouple measurements. Heated air was flown through the internal passages while the thermocouples read the actual surface temperatures and infrared camera was recorded the transient temperatures simultaneously. This procedure made sure that the calibration was performed for the entire range of expected temperature variation for an actual experiment. With such data, infrared camera output at each pixel location was readily converted to temperatures which eliminated the need to determine the surface emissivity. Also, during this calibration procedure, the infrared cameras were rigidly mounted and oriented relative to the vane in the same way as when the final experiments were run. This ensured that the variation in camera adjustment was not a factor in calibration data.

As will be discussed later, the present technique relies on relative differences of temperature between parts and not on absolute values. Thus, so long as the experimental test conditions—for example, ambient and inlet temperatures, position and orientation of camera and vanes—do not vary significantly, the differences would not be dependent on

the calibration procedure. This is another important differentiator which greatly impacts the usefulness of the present technique.

CHAPTER 3

3.1 Airflow Evaluation

As has been noted in section 2.4, air flow rates have been computed when the vane inlet temperatures reach a steady value. This also means that in this steady period the pressure at the inlet would remain constant, as shown in Figure 11 for both the pressure ratios tested. Effectively, this procedure allows us to capture any flow difference in an accurate and rigorous manner.

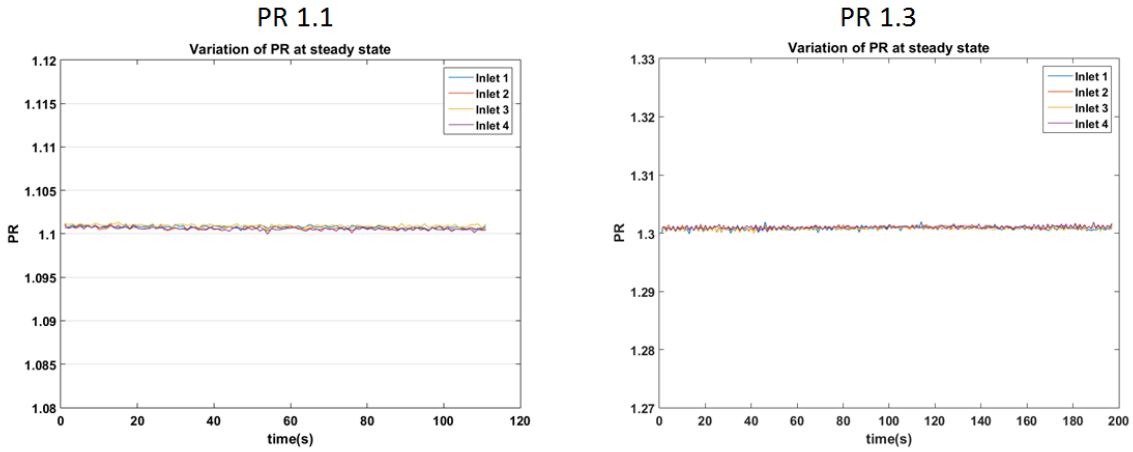

Figure 11: Variation of PR at the vane inlet at steady state

Air flow rate comparisons have been made based on the airfoil effective area (ACd) calculation—this is because effective area is a measure of flow capacity that is independent of local ambient conditions. Its calculation is based on the steady flow assumption for sub-critical isentropic flow at constant ambient pressure (Jia and Wang 2001), as shown in equation 2.

$$ACd = \frac{\dot{m}}{P_T\sqrt{\frac{2\gamma}{RT(\gamma-1)}}\sqrt{PR^{-\frac{2}{\gamma}} - PR^{-\left(\frac{\gamma+1}{\gamma}\right)}}} \quad (2)$$

where:

$\dot{m}$ = mass flow rate

ACd = effective area

PR = pressure ratio at inlet

P_T = total pressure at inlet

R = universal gas constant

γ = ratio of specific heats (c_p/c_v)

First, the air flow rate is calculated, using equation 1, based on the local ambient conditions. Once the airflow rate is known, equation 2 is used to compute effective area, ACd.

3.2 Comparison of air flow data (ACd)

Figure 12 shows the variation in ACd for OEM and repaired parts at 1.1 pressure ratio. A total of 8 OEM vane cluster, i.e., 32 airfoils and similarly 8 repaired vanes, or 32 repaired airfoils were tested, as shown on the horizontal axis of the figure. The average repaired airfoil flows 0.5% higher than the average OEM airfoil. The lowest flowing repaired airfoil was 1.37% lower than the lowest flowing OEM while the highest flowing repaired was 0.49% higher than the corresponding OEM airfoil.

In the case of PR 1.3, shown in Figure 13, the average repaired airfoil flows 1.2% higher than the average OEM airfoil. The maximum and minimum flowing repaired airfoils flow by 1.59% higher and 6.19% lower compared to the corresponding maximum and minimum flowing airfoils of the OEM group.

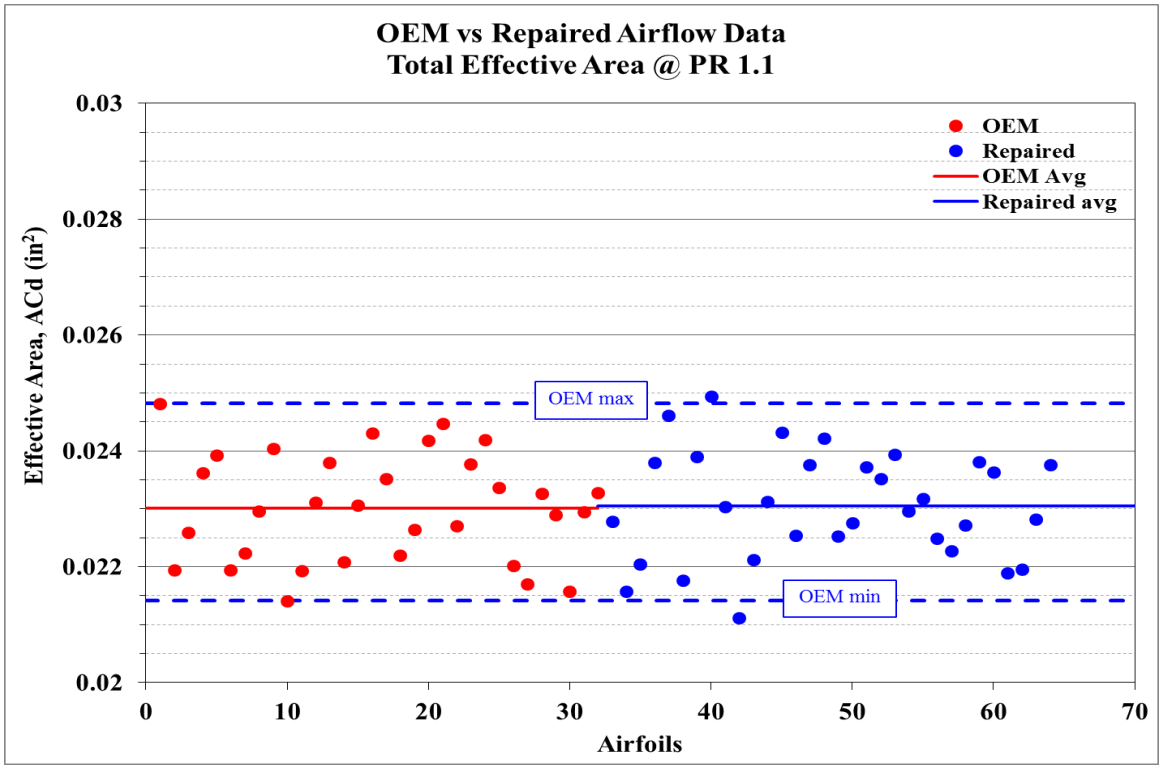

Figure 12: Comparison of ACd data between OEM and repaired parts at PR 1.1

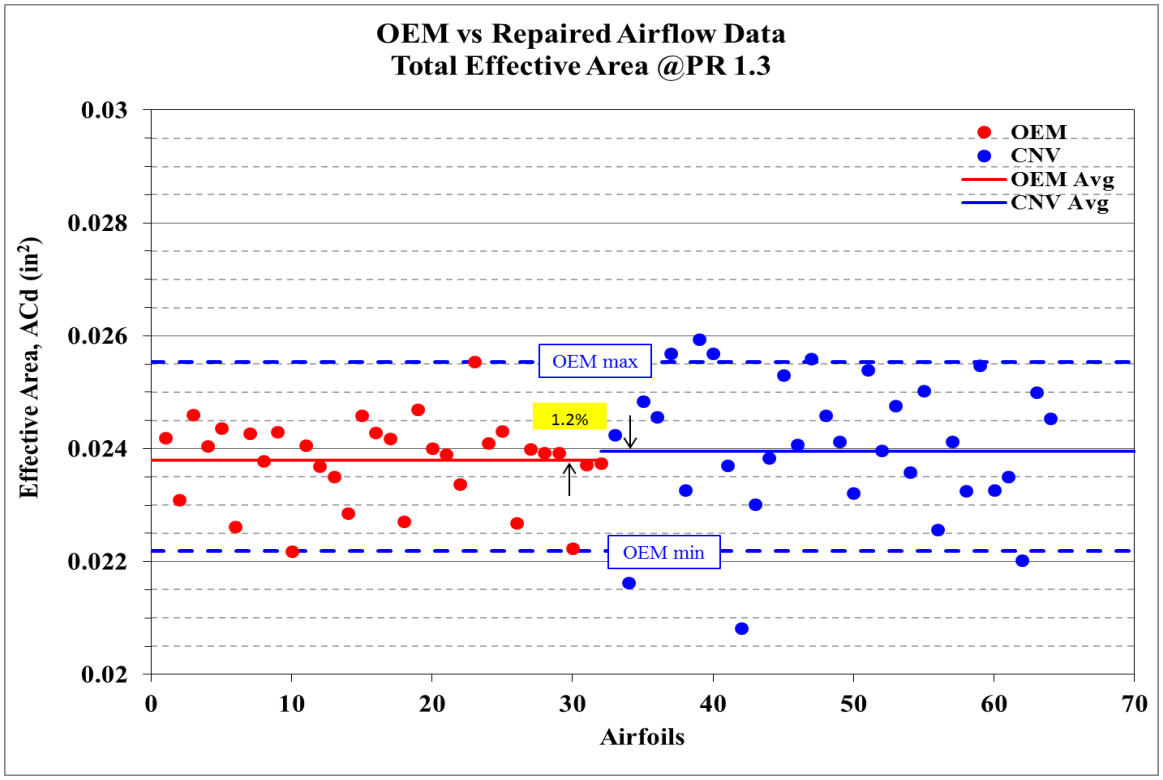

Figure 13: Comparison of ACd data between OEM and repaired parts at PR 1.3

Finally, a comparison of the individual airfoils of the OEM and repaired parts at both pressure ratios is presented in table 3. As evident from the table, the maximum/minimum deviation for any airfoil in the repaired parts sample from the OEM sample bound is within ±6%. The reader is reminded that although the present technique is aimed at evaluating differences in performance in individual airfoils, an important point to remember here is that, this amount of variation in air flow rates is expected. In total there are close to a hundred such airfoils per engine assembly with OEM and repaired vanes intermixed (there is a restriction on the maximum number of repaired vanes that can be present per engine assembly). As such, such small variations in air flow rates are expected to be offset by other airfoils which are high flowing. Of course, quantifying the extent to which such variations do not have an impact on the overall performance needs to be addressed. However, airflow variations can not only lead to discrepancies in the airfoil itself, but also in downstream components, which were not part of the test rig and is beyond the scope of the present study.

	PR 1.1				PR 1.3			
	Airfoil 1	Airfoil 2	Airfoil 3	Airfoil 4	Airfoil 1	Airfoil 2	Airfoil 3	Airfoil 4
OEM max	0.025	0.023	0.024	0.024	0.024	0.023	0.026	0.024
Repaired max	0.025	0.023	0.024	0.025	0.026	0.024	0.026	0.026
% higher	-0.8%	1.1%	0.5%	2.3%	5.4%	3%	1.6%	5.8%
OEM min	0.023	0.021	0.022	0.023	0.024	0.022	0.024	0.024
Repaired min	0.022	0.021	0.022	0.022	0.024	0.021	0.023	0.023
% lower	-4.3%	-1.4%	1.6%	-2%	0%	-6.2^	-2.9%	-4.7%

Table 1: Summary of variation in effective area (in^2) between OEM and repaired parts

Furthermore, the upper and lower limits in the present study are based on the average, maximum and minimum flows of the 8 tested OEM parts. Thus, the constructed maximum and minimum bounds are not sacrosanct – testing a large set of OEM parts should, therefore, broaden the bounds. Figure 14 shows the mean ACd for OEM and repaired parts and respective standard error of mean for both pressure ratios. In fact, a 95% confidence interval of the difference of means of OEM and repaired parts includes zero, which means that statistically the two sets of data, for both pressure ratios 1.1 and 1.3, cannot be differentiated—it is no different than saying that the datasets are samples from the same population.

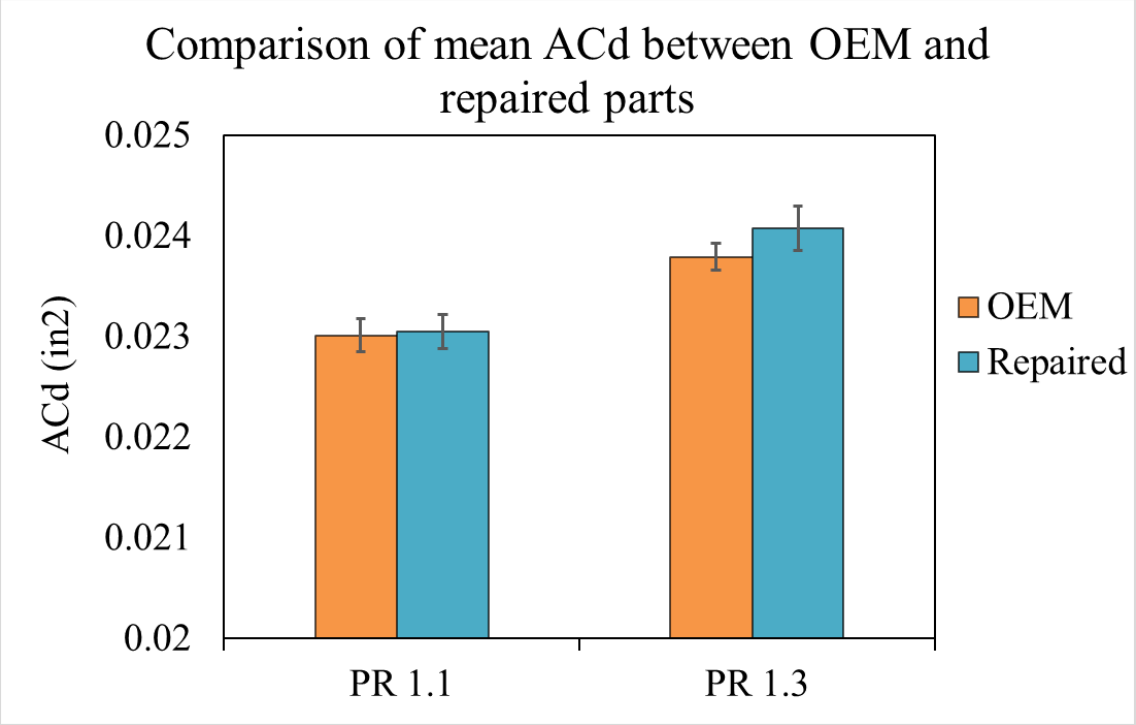

Figure 14: Mean ACd variation between OEM & repaired parts with their respective SE's

CHAPTER 4

4.1 Vane thermal performance characterization

Having compared the air flow data between the repaired and OEM parts, the next step was to formulate and characterize airfoil thermal performance. First, however, the impact of internal air flow on the vane surface temperature and consequently, the overall system needs to be appreciated with the present testing scheme. The infrared camera provides a map of the vane surface temperature—this can be used to locate any hotspots in the vane surface, if present, in a straightforward manner. Further, using a more involved analysis discussed later, the vane surface temperature can be used to compute a parameter comparing the thermal performance of the airfoils. This parameter can additionally be used to comment on the temperature of the air leaving the airfoil ID ports which can provide useful information regarding the health of components further downstream in the cooling path.

Before diving into the formulation of the parameter comparing airfoil heat transfer performance, we need to appreciate why just comparing the raw surface temperatures provided by the IR camera software was not desirable. For the direct one-to-one surface temperature comparison of an OEM and repaired vane to work, conditions like the inlet temperatures should match for the 2 vanes. Due to a number of reasons already discussed, however, not least because of the geometrical variations between repaired and OEM parts which impact the pressure drop and hence the flow rate, the inlet temperatures do not match exactly. Thus, to be certain of making an apples-to-apples comparison, it becomes rather important to normalize the surface temperatures of the vane using some realistic factor. Moreover, normalizing the surface temperature also negates the effect of small variations in the inlet temperatures among the airfoils of a single vane cluster and thus was a more robust technique of making comparisons as has been discussed in above. These intra-vane variations arise since the separate lines feeding these airfoils have slightly different heat losses due to the small differences in bends and pipe length, which was unavoidable.

Comparing normalized surface temperature, thus, provides us an opportunity to create a robust and consistent way of comparing airfoil thermal performance.

To reiterate, for the experiments performed in this study, data was captured after the heaters were powered off. This meant that the vane inlet and surface temperatures kept dropping gradually from a maximum, albeit different, values at the start of the experiment. Clearly, the path of heat transfer is from the hotter air inside through the vane to the ambient.

The proposed parameter used for analysis in this study was calculated using the formula below:

$$T^* = \frac{T_{vane(x,y)}(t) - T_{amb}}{T_{inlet}(t) - T_{amb}} . \frac{1}{\Delta T_v} \quad (3)$$

where:

$$\Delta T_v = \frac{T_{vane(x,y)(t_0)} - T_{amb}}{T_{inlet(t_0)} - T_{amb}}$$

$T_{vane(x,y)}(t)$ = surface temperature at location (x,y) of the vane at any time instant 't'.

T_{amb} = ambient temperature

t_0 = initial time

Before we consider what the term T* signifies, it would serve our understanding better if we unpack the individual terms appearing in the formulation of T* and notice how each behaves. Figure 15 shows the variation in airfoil inlet temperature and the surface temperature at two arbitrary points on two separate airfoils of the same 4-vane cluster during an experiment. Not surprisingly, these temperatures decrease from the start of the experiment when the heaters are powered off. However, the rates at which these temperatures drop—slope of the curves—are different. After powering off the heaters, essentially the cooler air from the main compressor is flowing through the circuit. However, due to the thermal inertia of the system, the air reaches the vane inlet picking up heat along the way starting from the heater exit. Hence, instead of a sharp decrease in inlet

temperature, we see a gradual decline. The vane surface, on the other hand, is losing heat to the ambient by radiation and natural convection while still absorbing heat from the same air flowing through the internal passages by virtue of the internal air being at a higher temperature than the surface temperature. The rate of drop in surface temperature, as seen in the figure, is still more gradual. If we were to extend the plot in Figure 15 further, beyond a point the inlet temperature would fall below the vane surface and the direction of heat transfer would reverse after this point. The time duration to this inflexion point is highly system dependent. In the development of the present technique, results have been computed for a stipulated time during which the internal temperature never fell below the vane surface temperature.

Now, simplistically, T* can be visualized to be the response of the vane (surface temperature) to a stimulus (inlet temperature) multiplied by a constant factor.

$$T^* = \frac{response_{(x,y)}}{stimulus} * constant\ factor$$

If the system were ideal, the response would follow the stimulus without any lag. For a unit drop in inlet temperature, the surface temperature would drop by an equal amount. However, in reality, resistance is provided to the flow of heat by the vane material and there is an associated thermal capacity. This means that at any point in time, because of the thermal resistance and heat capacity, there will be a difference in inlet and surface temperatures—otherwise, there would be no heat transfer from the internal air to the surface. Also, as has been discussed, the rates at which the inlet and surface temperatures drop will be different, thus, leading to a lag in what has been visualized here as response. Besides, without any loss of generality, the role of the constant factor, $1/\Delta T_v$ is to just force the parameter T* to begin from 1 at the start of the experiment.

Thus, we can infer, the more closely a point in the airfoil (response) follows the inlet temperature (stimulus), the lesser the lag and consequently, the closer the value to T* to 1. More the lag, higher is the variation from the forced value of 1 at the start. It is however, important to point out that the intent of the preceding discussion is not to classify an airfoil as good or bad based on the absolute T* value. Rather, it will be used to draw

comparisons between the repaired and OEM vanes—T* value for repaired vane relative to the T* value for OEM vane is what we are looking for.

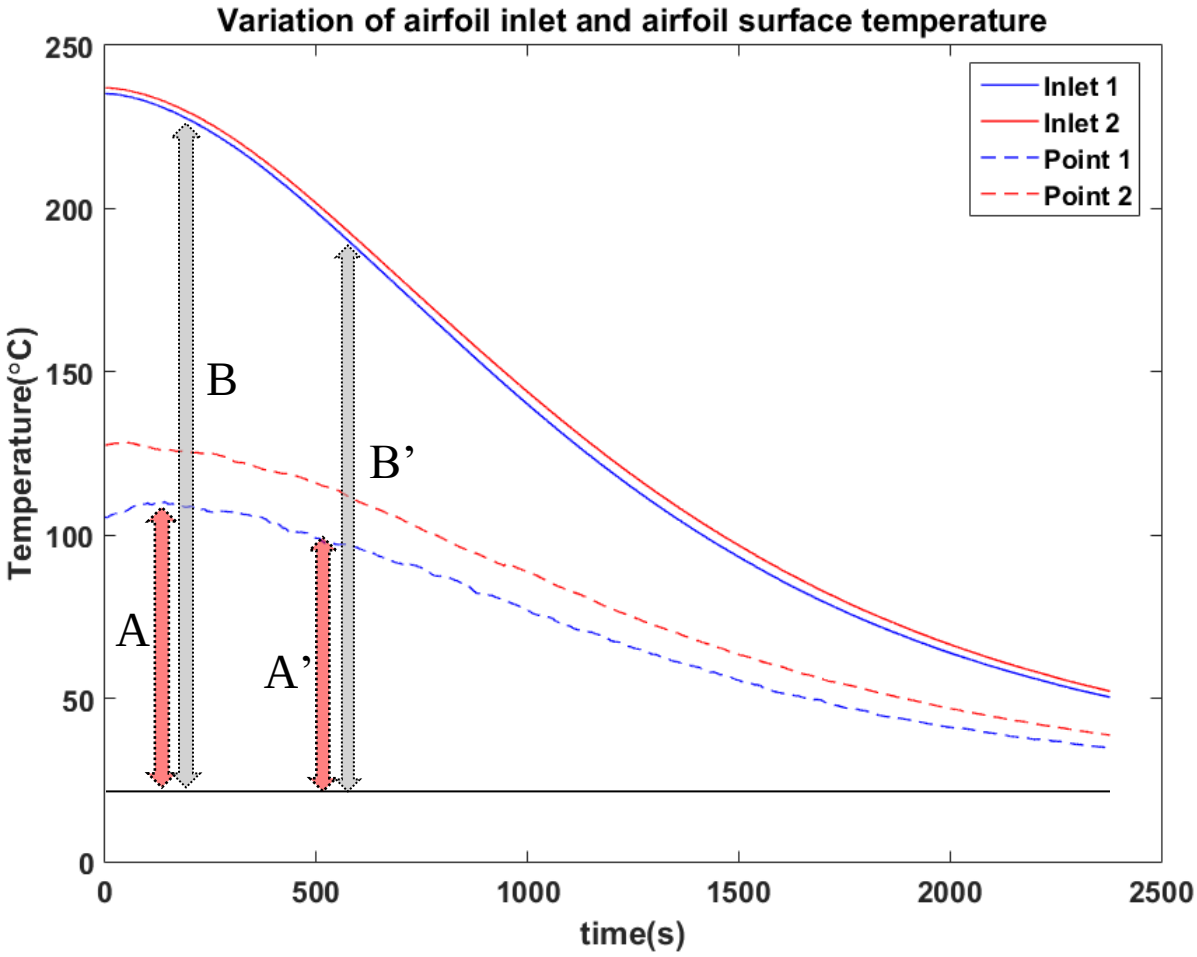

Figure 15: Variation in airfoil inlet temperature vs airfoil surface temperature for a test run

Figure 16 below shows the variation in the computed T* values for 2 arbitrary points against normalized time, where 0 signifies the start of the experiment and 1 the end. As expected from the analysis in the preceding paragraphs, the T* value starts at 1 and because of the lag in surface temperature response, it stays above the T* = 1 line for the most part. Another way of visualizing the variation of T* over normalized time is to consider two time instants, t1 and t2 (t2 > t1) in Figure 15. As has been discussed before, comparatively, rate at which inlet temperature drops is more than that of vane surface temperature as seen in Figure 15. The numerator of the T* formulation, therefore, increases

with elapsed time—A'/B' > A/B. This explains the variation seen in Figure 16. Again, this variation is highly system and test procedure dependent and should not be considered universally true. Depending on the thermal mass of the system, different variations might result. However, the comparison is based on the relative variation of the thermal performance characteristic and not on the absolute trend. It is, therefore, a legitimate characterization procedure.

Clearly, a point with higher heat transfer characteristics (T* close to 1) compared to another point will have a smaller area under its curve. That is, integrating T* over time will yield a smaller value for a point whose response follows the stimulus more closely. Effectively, therefore, the entire temporal response of a point in the airfoil can be reduced to a single value: the area under the T* curve. This does not, however, mean that the point showing more lag (larger area under the curve) is problematic. In a real engine, different locations on the airfoil see different external air temperature loads. For example, the leading edge sees the highest temperatures and as such needs better cooling. As such, what is important for us to compare is not the individual integral T* values of points on the airfoil; rather, how the area-averaged integral T* value over a repaired airfoil compares to the same integral T* value of a corresponding OEM airfoil. This data in presented in the charts of the next section.

Another conclusion that can be drawn from comparing the area-averaged integral T* values is regarding the temperature of the air leaving the airfoil ID ports and flowing into the disc cavity. Assuming we are comparing 2 4-vane clusters having equal air flow rates, if the thermal performance of these 2 vanes were similar, the air flowing through the internal cavities of these vanes would end up exchanging roughly equal amounts of heat, given that the mass flow rates are equivalent. Therefore, if the air inlet temperatures to these vanes were similar, other conditions being consistent, the temperature of the air leaving these vanes would be in the same ballpark range.

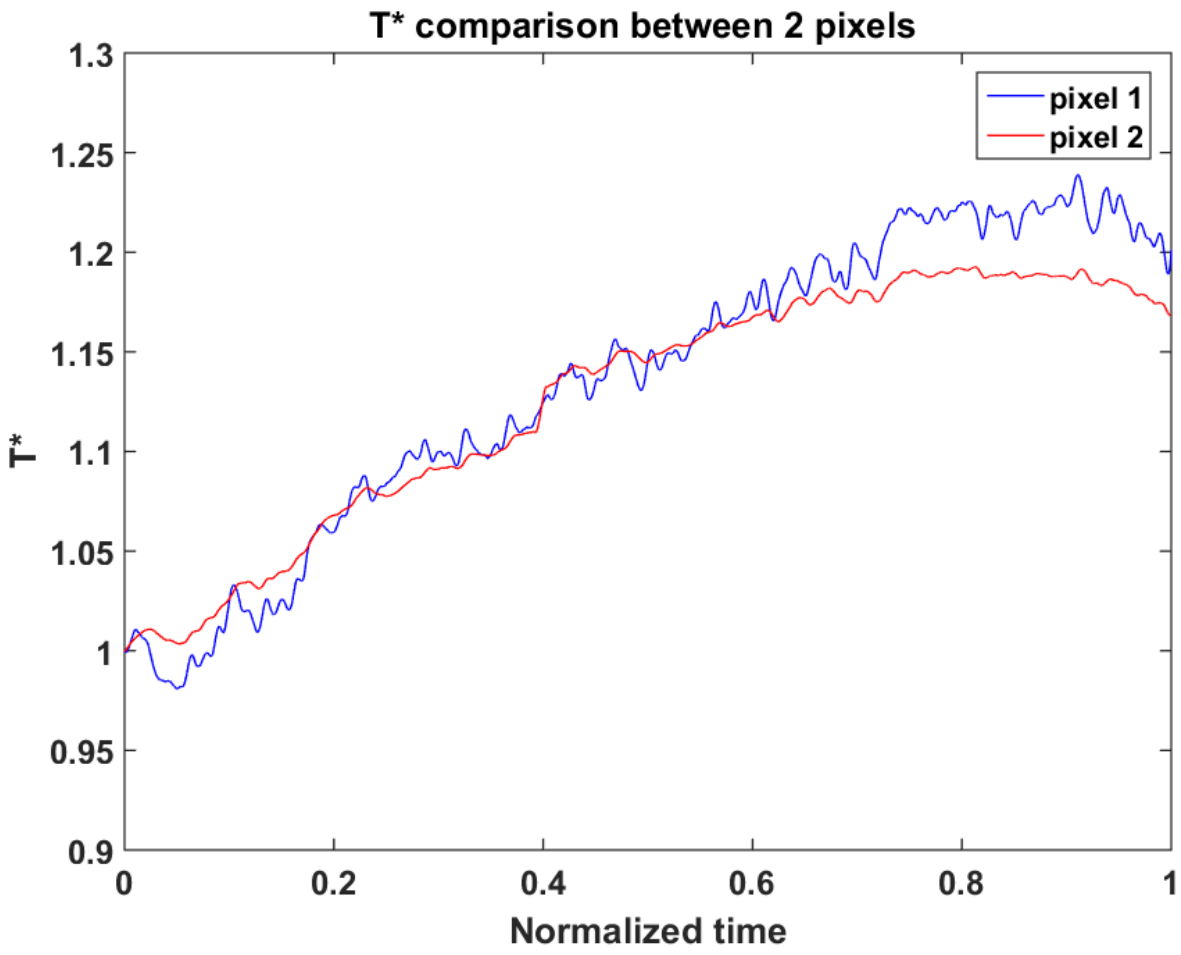

Figure 16: Variation in the parameter T* for 2 points on a vane

4.2 Comparison of integral T* values

As in the case of comparing ACd data, a similar kind of chart is presented for comparing integral T* values between the repaired and OEM parts. Airfoils (32 OEM airfoils and 32 repaired airfoils) are on the horizontal axis while their corresponding area-averaged integral T* values on the vertical axis.

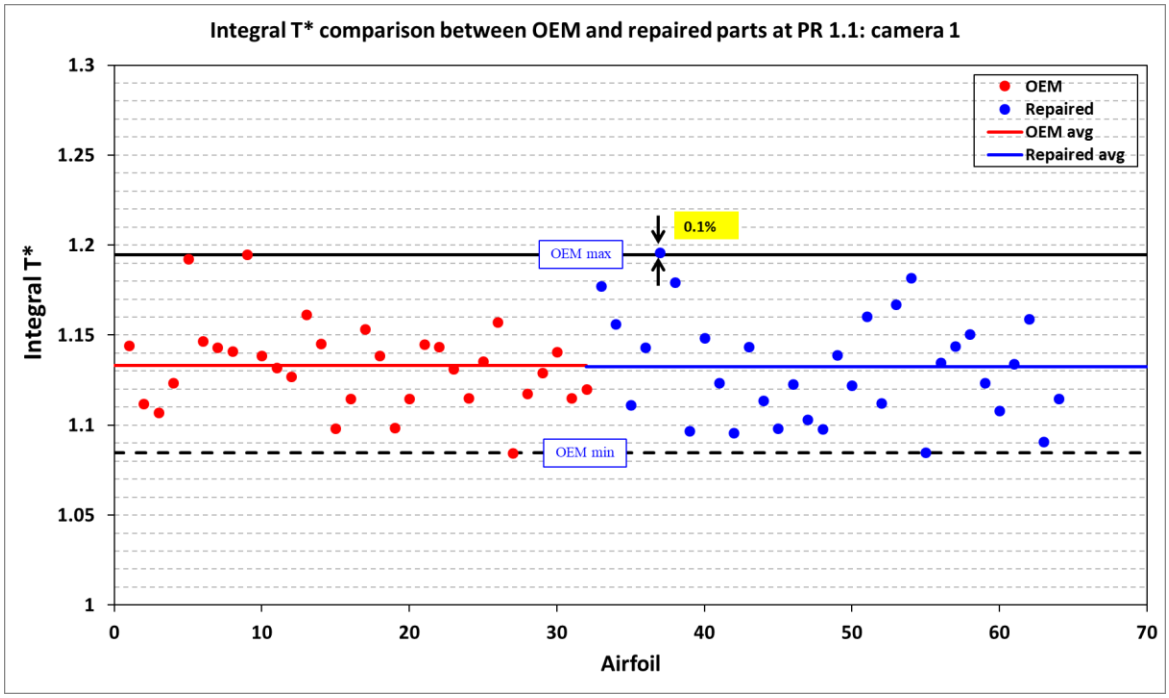

Figure 17: Comparison of area-averaged integral T* values between OEM and repaired parts at PR 1.1 for camera 1

Figure 17 shows a comparison of the area-averaged integral T* values between the repaired and OEM parts at 1.1 PR for the 1st camera looking the suction side of the airfoils. As can been seen, hardly any difference was observed between the two sets—the overall average integral T* values, as well as the maximum and minimum integral T* values, are quite similar for both the sets. In the case of camera 2, which was viewing the pressure side of the vanes, the integral T* average, shown in Figure 18, for the OEM airfoils was lower by 0.43% compared to the repaired airfoils. Even though quite a few of the airfoils (~40%) are outside the range of integral T* values evaluated for the OEM vanes, the maximum and minimum deviations are only 2.32% and 0.5% respectively.

Again, it is worth reiterating that the range shown in the figure for OEM parts is based off only the 8 vanes or 32 airfoils that were part of the test and as such these are not hard limits. Moreover, considering the fact that there are 96 airfoils in a real engine assembly at a particular stage with OEM and repaired parts intermixed, these variations are expected to have a minimal effect on the thermal performance of the system as a whole, especially the impact on downstream cooling path components. Besides, having created

the bounds on integral T*, this technique provides us with clues on which vane could be the problematic one. A detailed study with larger number of OEM and properly functioning repaired parts will be beneficial in characterizing the bounds and thus enabling us to pinpoint a faulty vane based on integral T* results. Another important benefit of this thermal performance characterization that can be utilized will be in intermixing vanes in an assembly based on their integral T* values. A batch of vanes having higher than average integral T* vanes can be mixed with another group having lower than average values, thus averaging out the impact of each sub-group. In effect, it would help the manufacturer in using more built parts, reduce waste, and provide better control.

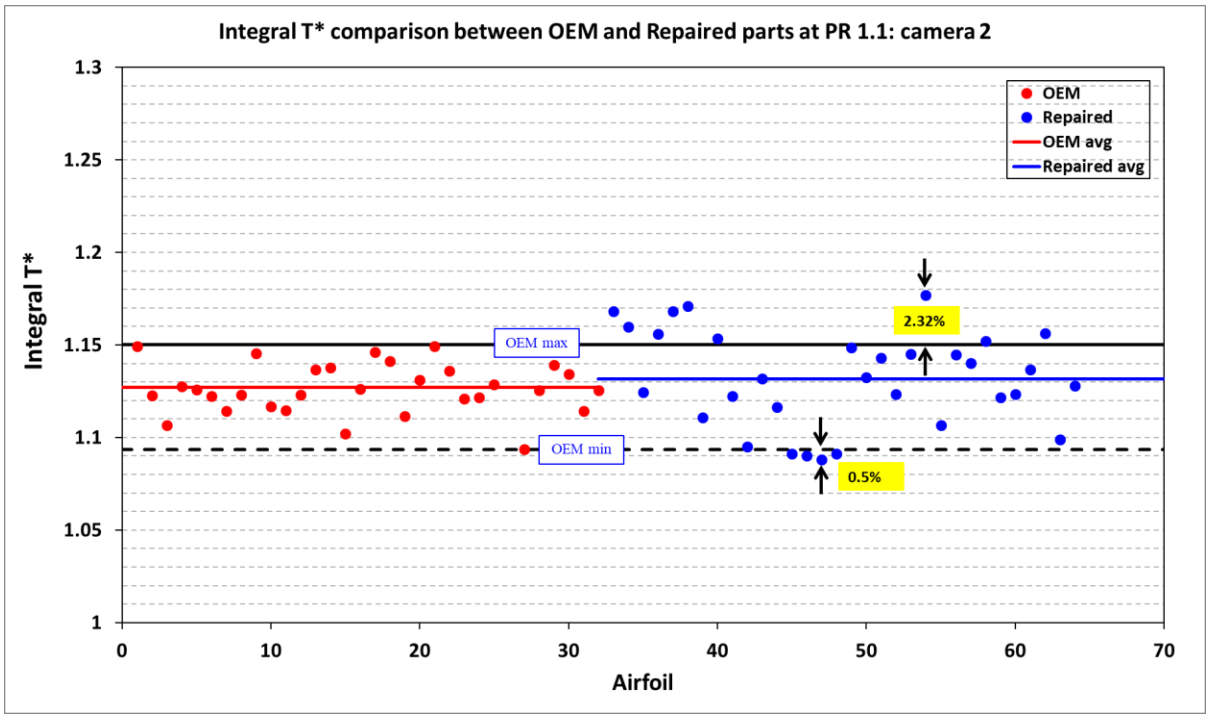

Figure 18: Comparison of area-averaged integral T* values between OEM and repaired parts at PR 1.1 for camera 2

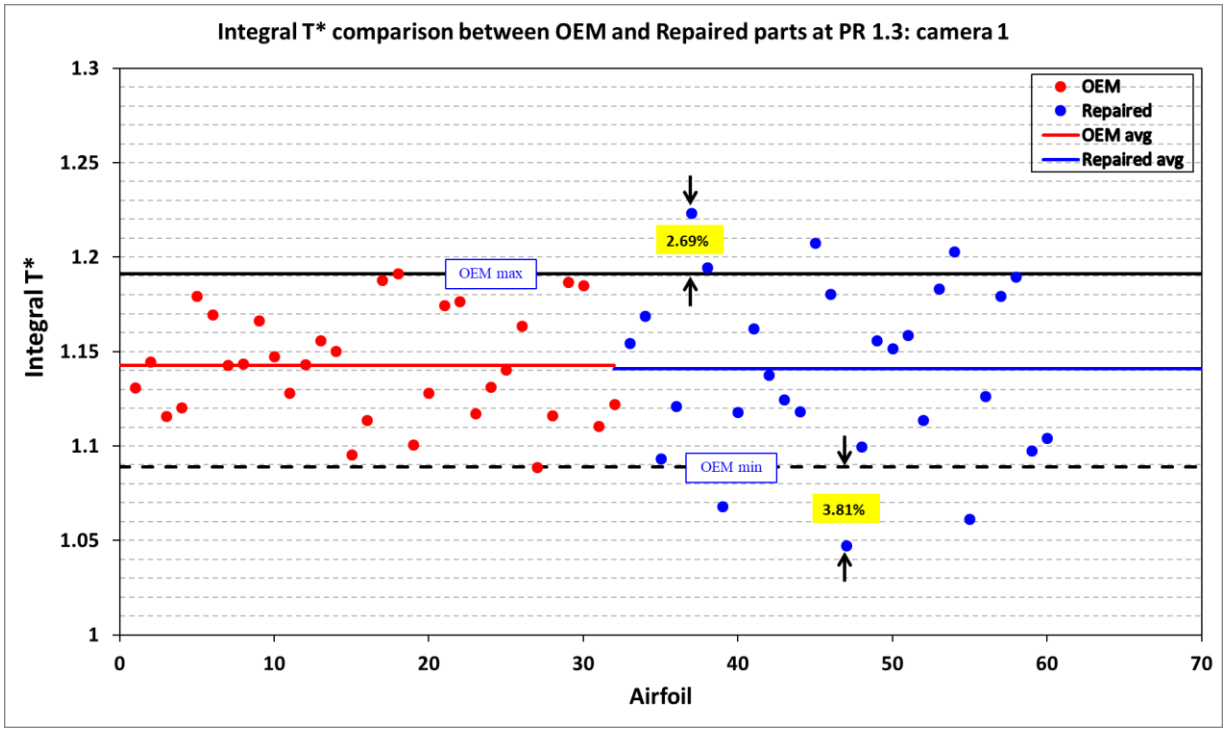

Figure 19: Comparison of area-averaged integral T* values between OEM and repaired parts at PR 1.3 for camera 1

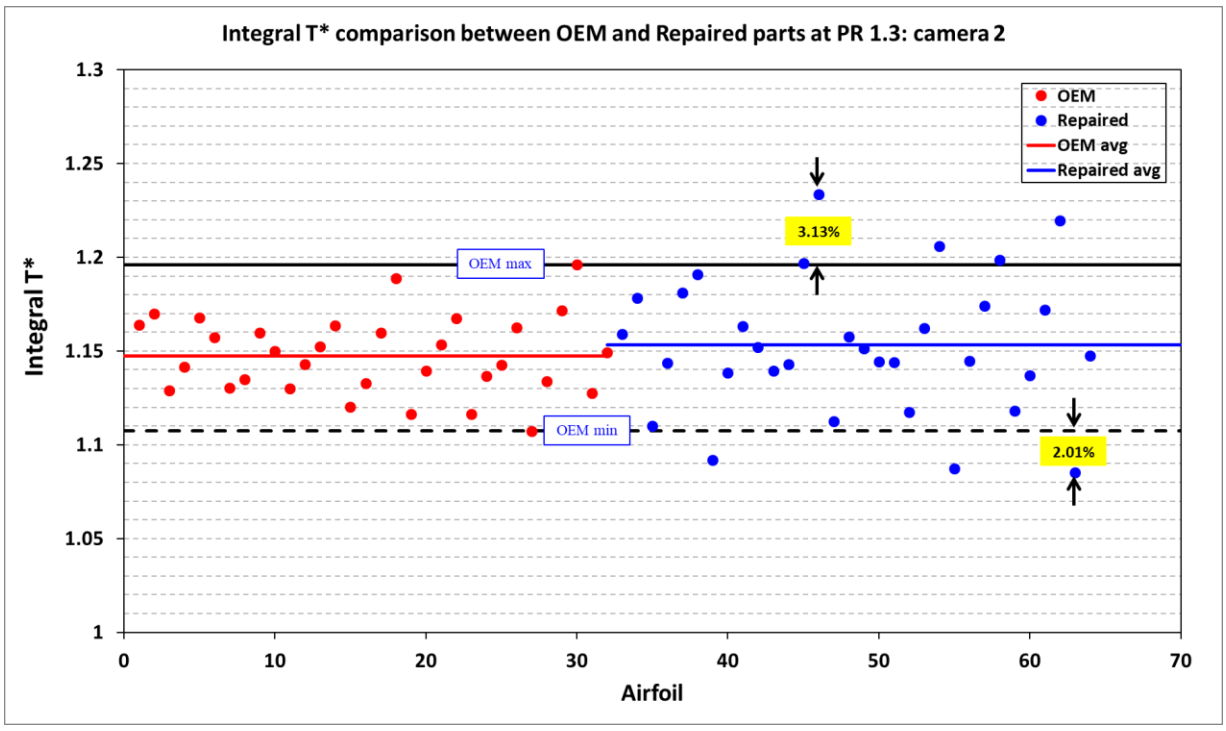

Figure 20: Comparison of area-averaged integral T* values between OEM and repaired parts at PR 1.3 for camera 2

Similarly, the results for area-averaged integral T* values at PR 1.3 are shown in Figure 19 and Figure 20. The results are similar to what has been observed at 1.1 PR. Average integral T* values for camera 1, which is viewing the suction side of the vane, differs by only 0.16%. While the average integral T* value for camera 2, viewing the pressure side, was 0.51% higher for OEM airfoils compared to repaired airfoils. The maximum and minimum deviations of the repaired airfoils are within 4% from the observed OEM bounds.

Figure 21 and Figure 22 show the mean integral T* for OEM and repaired parts and respective standard error of mean fosr both pressure ratios. Again, like what was observed with mean ACd values, a 95% confidence interval of the difference of means of OEM and repaired parts includes zero. This is equivalent to saying that the null hypothesis (that any two corresponding samples, say OEM vs Repaired for PR 1.1 and camera 1, have the same mean) cannot be rejected at the significance level, α, of 5%.

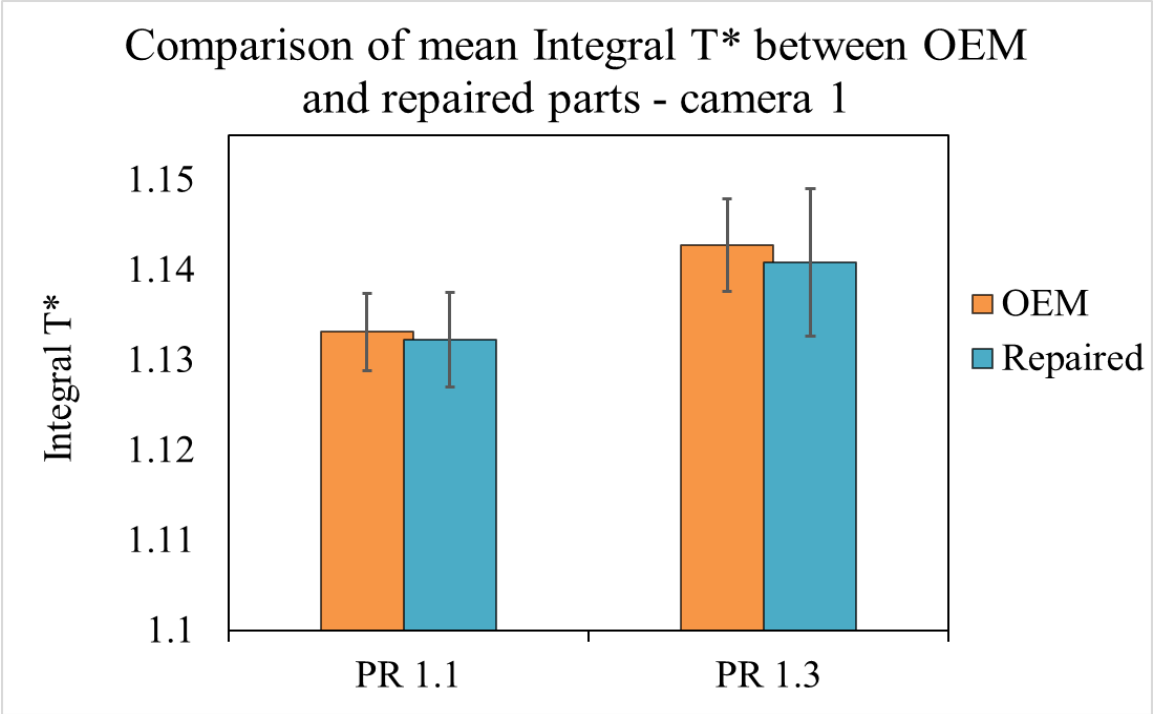

Figure 21: Integral T* comparison between OEM and Repaired parts for camera 1

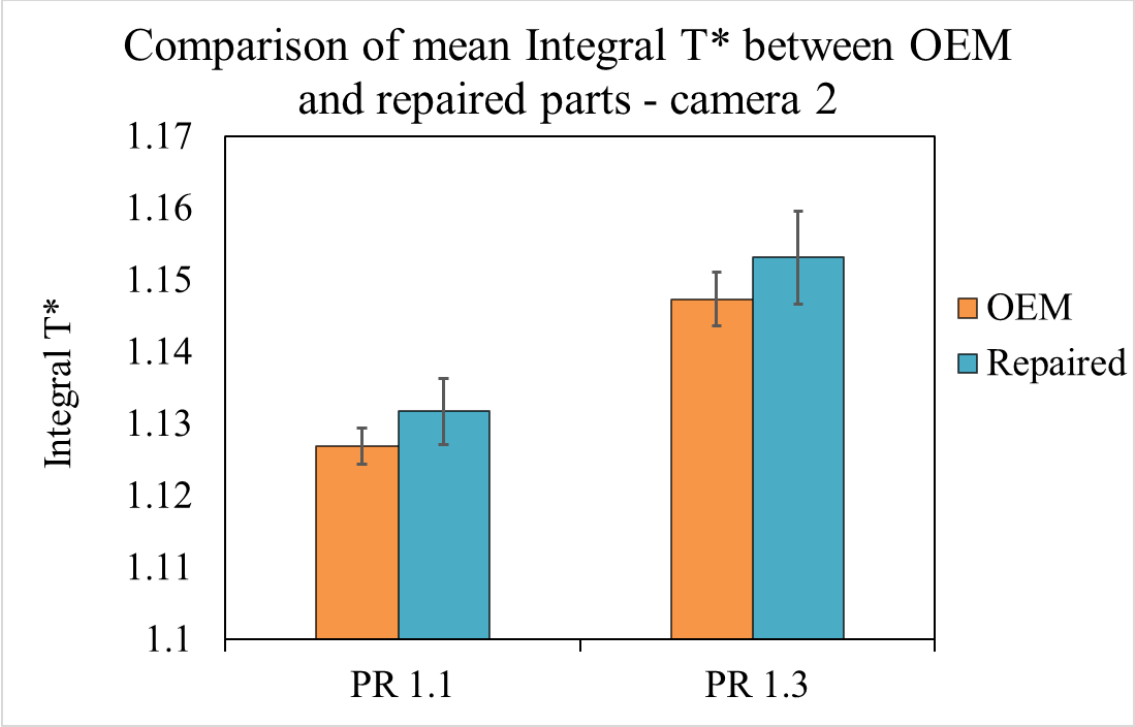

Figure 22: Integral T* comparison between OEM and Repaired parts for camera 2

It is, however, clear from the above plots that the spread in the repaired vane samples are larger compared to OEM vanes. As has been discussed, the number of airfoil samples is quite small and the spread of ACd or integral T* values of the whole OEM population will be larger than the current sample tested. Besides, looking at Figure 19 or Figure 20 one gets the impression that the thermal performance of the repaired parts are outside bounds even though the deviations are quite low. A low deviation, however, may not amount to being insignificant. An attempt has been made below to statistically verify the possibility of obtaining these seemingly outside of bound values.

Now, to predict the range of population variation from the OEM samples of integral T* we need to know the inherent distribution of the samples. Based on random variations on part manufacturing it is expected that the population will be normally distributed. This can be verified by using the normal probability plot, as shown in Figure 23. For a distribution that is approximately normal, the data points (blue circles) look as if they form a straight line. Referring Figure 23, it is clear that the integral T* population for both cameras and pressure ratios are approximately normally distributed although deviations from the straight red lines are observed at the extremes. This is usually associated with

having wider or narrow distributions compared to an arithmetic normal distribution. However, for the present case of drawing inference, assuming an underlying normal distribution should be sufficient.

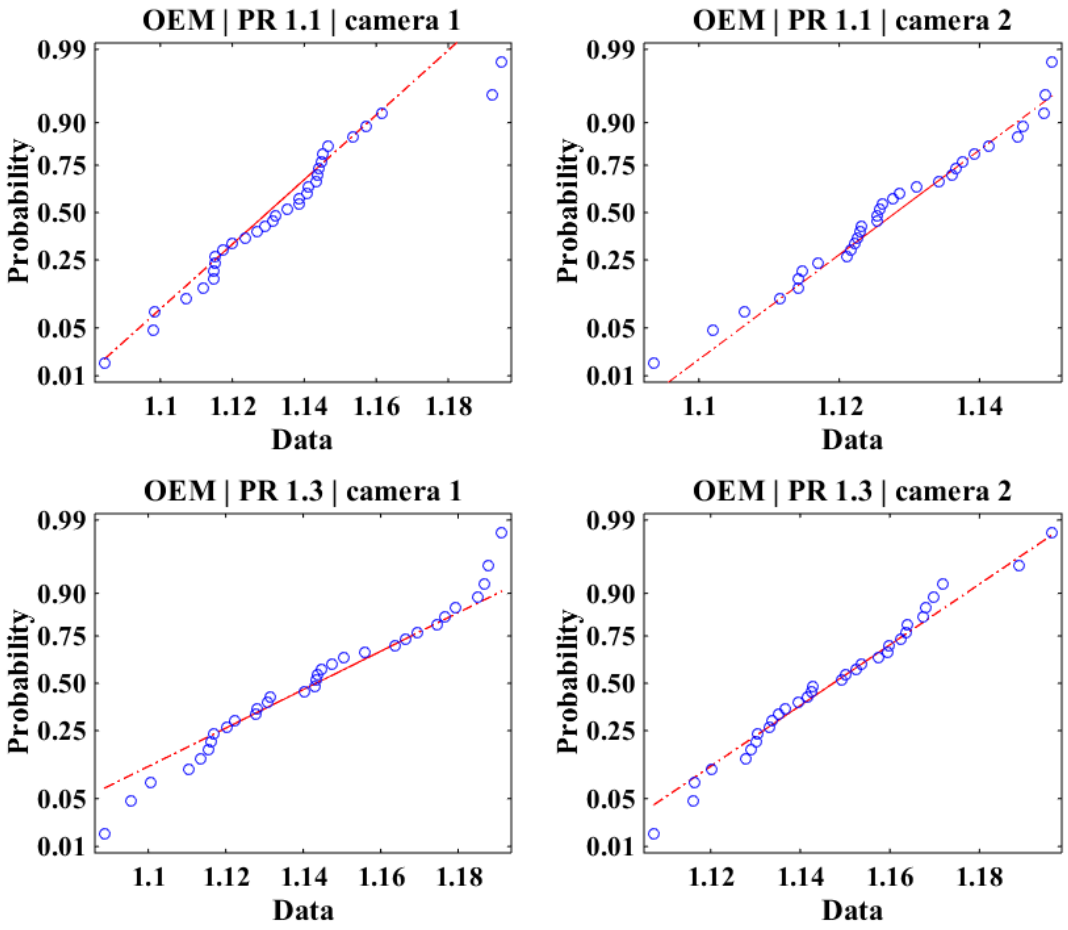

Figure 23: Normal probability plot of Integral T* values for both cameras at both PRs

Based on the above information, a reference range of integral T* population variation in OEM parts can be constructed. Since only the sample standard deviation is known, a t-score was used for the calculation of the reference range. A 95% reference range can be calculated as (mean ± 2*sample standard deviation). A multiplying factor of 2 was used because for large sample size ($n \geq 30$), the 97.5% quantile of a Student's t-distribution with n-1 (where n is sample size) degrees of freedom, $t_{0.975,n-1,}$ can be approximated as 2. Now, there is an uncertainty associated with the reference range predictions as well and the reference range limits will themselves have a confidence interval. Because the underlying

distribution is approximately normal as has been demonstrated, the formula below can be applied to find the 90% confidence interval (CI) of the standard reference range (SRR) limit.

$$LL\ of\ the\ CI\ of\ the\ LL\ of\ the\ SRR = LL\ of\ SRR - 2.81 * \frac{SD}{\sqrt{n}}$$

$$UL\ of\ the\ CI\ of\ the\ LL\ of\ the\ SRR = LL\ of\ SR + -2.81 * \frac{SD}{\sqrt{n}}$$

To summarize the above discussion briefly, it is expected that ~95% of the population would fall in between the calculated limits below:

Case	Lower limit	Upper limit
PR 1.1 & camera 1	1.0724	1.1939
PR 1.1 & camera 2	1.0916	1.1624
PR 1.3 & camera 1	1.0694	1.2161
PR 1.3 & camera 2	1.0944	1.2004

Table 2: Reference range of integral T* of OEM population

A graphical summary of the above discussion can be seen in Figure 24. The grayed out rectangular columns represent the calculated 95% OEM population bound, while the colored filled circles each represents an individual repaired airfoil at the corresponding pressure ratio and view. Clearly, the deviation of repaired parts from expected OEM reference range is further smaller than was seen in case for the OEM sample in Figure 17 through Figure 20.

Besides, the possibility of the repaired parts having a wider spread in thermal performance and still satisfying the requirements cannot be discounted either. To ascertain the accepted dispersion, a detailed study should be carried out by the party interested in repairing these parts and identify the limits irrespective of how much variation is observed compared to OEM parts. Solely tagging a part as ‘good’ or ‘bad’ based on comparison with

OEM bounds will not be prudent. However, the technique discussed in this report can be utilized to create these bounds separately for the repaired parts and thereafter use that for identifying faulty parts. The population means for OEM and repaired parts are still expected to be very close to one another as has been observed in the experiments performed during the development of the current technique.

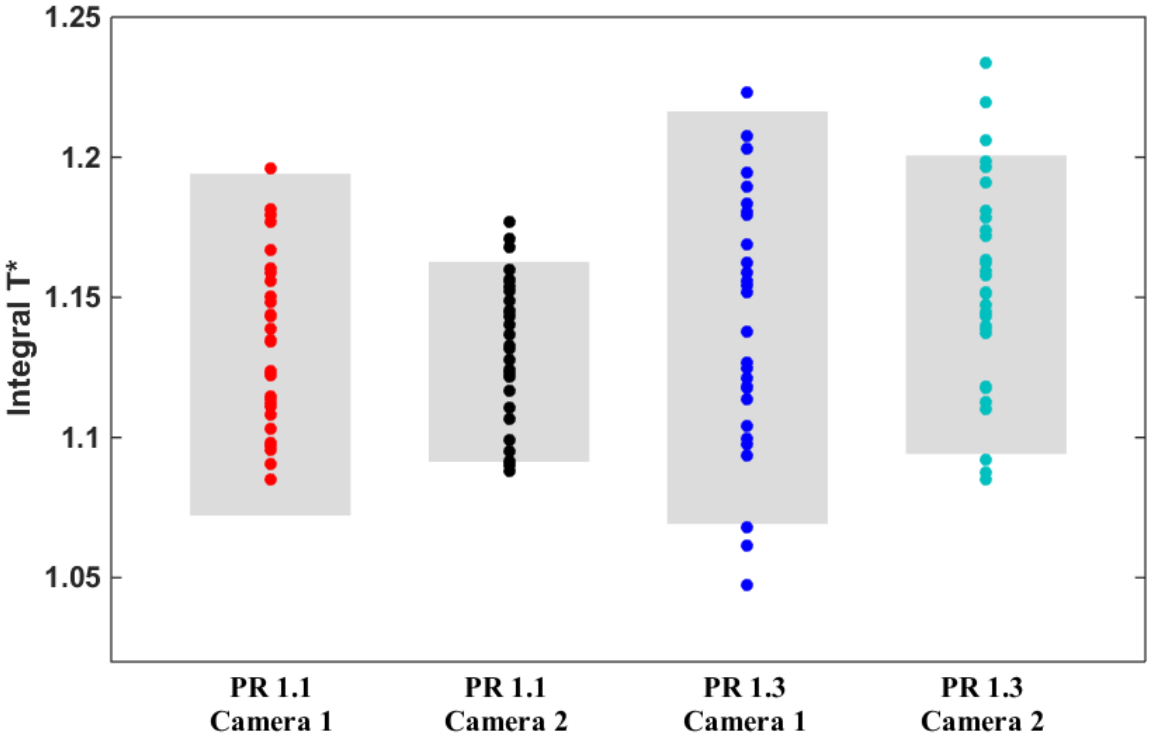

Figure 24: Comparison of integral T* variation of repaired parts with estimated 95% CI of OEM population range

CHAPTER 5

5.1 Conclusion

Experiments were performed to evaluate and understand the impact temperature has on the air flow rates and thermal performance of repaired vanes as compared to original equipment manufacturer (OEM) vanes. High temperature air at 250-300˚C was flown

through the internal passages of these vanes and mass flow rates and surface temperatures of the airfoils recorded. Measurements were taken at two different pressure ratios: 1.1 and 1.3, between the inlet to the vane and ambient. On average, it was found that the effective area (ACd) for repaired parts were higher by 0.15% and 1.2% compared to the OEM parts at pressure ratios 1.1 and 1.3 respectively. These differences, however, were not found to be statistically significant at 95% confidence level. The majority of the ACd values of individual airfoils fell within the range of values found for the OEM parts. In addition, the surface temperatures of the heated vanes were measured using infrared thermography. A parameter, named T*, was developed to compare the thermal performance of the vanes. Comparisons in thermal performance were made based on the area-averaged time-integral values of this parameter, T* which is a way of representing the thermal behavior of an airfoil for the entire duration of an experiment using a single data point. At the individual airfoil level, a maximum deviation of 3.81% was observed in repaired parts from the OEM maximum, for comparisons including both pressure ratios and viewing surface. The average integral T* values for all the vanes, on the other hand, showed very small variations similar to what was observed for the average ACd data. Using statistical analysis it was verified that the mean difference between the OEM and repaired samples for integral T* was not significantly different either. Some excursions from the calculated OEM population bounds were observed for a few of the repaired airfoils, however, it was realized that such deviations do not necessarily point to a defective part. Overall, the sensitivity of the developed technique was found to be high which means that once a robust set of data is acquired, identification of defective parts would be highly streamlined. The robustness of the current technique borne by the use of a normalizing parameter to negate the variability in test rig, operating and ambient conditions will help manufacturing companies to reduce costs while still a maintaining high level of part screening procedure.

5.2 Future Work

The repaired parts evaluated for the development of the described technique were not known to have defects—it was, otherwise, a blind test. A logical progression to validate the developed parameter will be to test parts that are known to have defects and assess their

ACd and integral T* variation compared to the population bound. Further, a formal design of experiments analysis should be carried out to ascertain the test conditions that would result in minimum uncertainty. This will help in better control of the experiments and improve the statistical significance of the testing procedure further. Another important work, also pointed out in the section 4.2, is related to expected variation of thermal performance among repaired parts. Although the standard deviation of repaired parts sample was slightly higher in comparison to the OEM sample, does this larger spread mean that the repaired parts would perform poorly compared to the OEM parts? The processes involved in manufacturing the OEM and repaired parts vary not by an insignificant amount. As such, small variation in their thermal performance characteristics is not alarming. As long as reliability and function of the system overall is not sacrificed, minor deviations should be tolerable. Future studies should consider the spread of properly functioning repaired parts and compare it against those which are faulty. Analysis only based on comparing the repaired parts to their OEM counterparts might be short-sighted and result in misjudgment and incur losses to the organization.

REFERENCES

Antony, K.C., and G.W. Goward. 1988. “Aircraft Gas Turbine Blade and Vane Repair.” *Superalloys 1988 (Sixth International Symposium)*: 745–54. http://www.tms.org/Superalloys/10.7449/1988/Superalloys_1988_745_754.pdf.

Bantel, Thomas E. 1992. “Apparatus And Method For Inspecting Cooling Holes.” (0).

Bantel, Thomas E., and David C Mack. 1987. “Cooling Hole Inspection.”

Beckeiz, E, A Sperling, and V Carl. 1998. “Thermography Inspection System for Gas Turbine Blades.” *7th ECNDT, Copenhagen, Denmark*.

Bunker, Ronald S., and Jason R. Allen. 2010. “System And Method For Thermal Inspection of Parts.”

Bunker, Ronald S., and Nirm V. Nirmalan. 2011. “Thermal Inspection System and Method.”

Carter, Tim J. 2005. “Common Failures in Gas Turbine Blades.” *Engineering Failure Analysis* 12(2): 237–47.

Ekkad, Srinath V, and Je-Chin Han. 2000. “A Transient Liquid Crystal Thermography Technique for Gas Turbine Heat Transfer Measurements.” *Measurement Science and Technology* 11(7): 957. http://stacks.iop.org/0957-0233/11/i=7/a=312.

Han, Je-Chin, Sandip Dutta, and Srinath Ekkad. 2012. “Gas Turbine Heat Transfer and Cooling Technology.” 6: 1–30.

Han, Je Chin, and Akhilesh P. Rallabandi. 2010. “Turbine Blade Film Cooling Using PSP Technique.” *Frontiers in Heat and Mass Transfer* 1(1).

Harrold, Ronald, and Zal Sanjana. 2002. “Acoustic Waveguide Sensing the Condition of Components within Gas Turbines.” 2(12).

Ireland, P. T., Z. Wang, and T. V. Jones. 1993. “Liquid Crystal Heat Transfer Measurements.” *In VKI, Measurement Techniques 48 p (SEE N94-18643 04-35)*. http://adsabs.harvard.edu/abs/1993VKIMT.....I (February 12, 2018).

ISO, E N. 2003. “Measurement of Fluid Flow by Means of Pressure Differential Devices Inserted in Circular Cross Section Conduits Running Full—Part 2: Orifice Plates.” *EN ISO*: 5162–67.

Jia, L X, and L Wang. 2001. “Equations For Gas Releasing Process From Pressurized Vessels In ODH Evaluation.”

Maldague, X., F. Galmiche, and A. Ziadi. 2002. “Advances in Pulsed Phase Thermography.” *Infrared Physics and Technology* 43(3–5): 175–81.

Mazur, Z., A. Luna-Ramírez, J. A. Juárez-Islas, and A. Campos-Amezcua. 2005. “Failure Analysis of a Gas Turbine Blade Made of Inconel 738LC Alloy.” *Engineering Failure Analysis* 12(3): 474–86.

McGraw, Julie, George Van Deventer, Reiner Anton, and Andrew Burns. 2006. “Advancements in Gas Turbine Vane Repair.” *ASME 2006 Power Conference* 2006: 385–89.

Meola, Carosena, Giovanni Maria Carlomagno, Antonino Squillace, and Antonio Vitiello. 2006. “Non-Destructive Evaluation of Aerospace Materials with Lock-in Thermography.” *Engineering Failure Analysis* 13(3 SPEC. ISS.): 380–88.

Nirmalan, Nirm V, Ronald S Bunker, and Carl R Hedlung. 2003. “The Measurement of Full-Surface Internal Heat Transfer Coefficients for Turbine Airfoils Using a Non-Destructive Thermal Inertia Technique.” *Journal of Turbomachinery* 125(1): 83–89. http://link.aip.org/link/abstract/ASMECP/v2002/i36088/p365/s1%5Cnhttp://nir_measurementfullsurface02.pdf.

Park, Myounggu, Young Ha Hwang, Yun Seung Choi, and Tae Gu Kim. 2002. “Analysis of a J69-T-25 Engine Turbine Blade Fracture.” *Engineering Failure Analysis* 9(5): 593–601.

Powel, S F. 1991. “On the Leading Edge: Combining Maturity and Advanced Technology on the F404 Turbofan Engine.” *Journal of Engineering for Gas Turbines and Power* 113(1): 1–10. http://gasturbinespower.asmedigitalcollection.asme.org/article.aspx?articleid=1417913.

Ravi, Bharath Viswanath, Prashant Singh, and Srinath V. Ekkad. 2017. “Numerical Investigation of Turbulent Flow and Heat Transfer in Two-Pass Ribbed Channels.” *International Journal of Thermal Sciences* 112: 31–43. https://www.sciencedirect.com/science/article/pii/S1290072916304434 (February 12, 2018).

Shepard, Steven M. 2003. “Reconstruction and Enhancement of Active Thermographic Image Sequences.” *Optical Engineering* 42(5): 1337. http://opticalengineering.spiedigitallibrary.org/article.aspx?doi=10.1117/1.1566969.

Singh, Prashant, and Srinath Ekkad. 2016. “Effects of Rotation on Heat Transfer due to Jet Impingement on Cylindrical Dimpled Target Surface.” In *Volume 5B: Heat Transfer*, ASME, V05BT16A010. http://proceedings.asmedigitalcollection.asme.org/proceeding.aspx?doi=10.1115/GT2016-57145 (February 12, 2018).

———. 2017a. “Experimental Study of Heat Transfer Augmentation in a Two-Pass Channel Featuring V-Shaped Ribs and Cylindrical Dimples.” *Applied Thermal Engineering* 116: 205–16. https://www.sciencedirect.com/science/article/pii/S1359431117305471 (February 12, 2018).

Singh, Prashant, and Srinath V. Ekkad. 2017b. “Effects of Spent Air Removal Scheme on Internal-Side Heat Transfer in an Impingement-Effusion System at Low Jet-to-Target Plate Spacing.” *International Journal of Heat and Mass Transfer* 108: 998–1010. https://www.sciencedirect.com/science/article/pii/S0017931016331283 (February 12, 2018).

———. 2017c. “Experimental Investigation of Rotating Rib Roughened Two-Pass Square Duct With Two Different Channel Orientations.” In *Volume 5A: Heat Transfer*, ASME, V05AT16A012. http://proceedings.asmedigitalcollection.asme.org/proceeding.aspx?doi=10.1115/GT2017-64225 (February 12, 2018).

Singh, Prashant, Yongbin Ji, and Srinath V. Ekkad. 2018. “Experimental and Numerical Investigation of Heat and Fluid Flow in a Square Duct Featuring Criss-Cross Rib Patterns.” *Applied Thermal Engineering* 128: 415–25. https://www.sciencedirect.com/science/article/pii/S1359431117335664 (February 12, 2018).

Singh, Prashant, Yongbin Ji, Mingyang Zhang, and Srinath V. Ekkad. 2017. “Heat Transfer Enhancement by Criss-Cross Pattern Formed by 45° Angled Rib Turbulators in a Straight Square Duct.” In *Volume 1: Aerospace Heat Transfer; Computational Heat Transfer; Education; Environmental Heat Transfer; Fire and Combustion Systems; Gas Turbine Heat Transfer; Heat Transfer in Electronic Equipment; Heat Transfer in Energy Systems*, ASME, V001T06A003. http://proceedings.asmedigitalcollection.asme.org/proceeding.aspx?doi=10.1115/HT2017-4908 (February 12, 2018).

Singh, Prashant, Weihong Li, Srinath V. Ekkad, and Jing Ren. 2017a. “A New Cooling Design for Rib Roughened Two-Pass Channel Having Positive Effects of Rotation on Heat Transfer Enhancement on Both Pressure and Suction Side Internal Walls of a Gas Turbine Blade.” *International Journal of Heat and Mass Transfer* 115: 6–20. https://www.sciencedirect.com/science/article/pii/S0017931017318975 (February 12, 2018).

———. 2017b. “Experimental and Numerical Investigation of Heat Transfer inside Two-Pass Rib Roughened Duct (AR = 1:2) under Rotating and Stationary Conditions.” *International Journal of Heat and Mass Transfer* 113: 384–98. https://www.sciencedirect.com/science/article/pii/S001793101730162X (February 12, 2018).

Singh, Prashant, Jaideep Pandit, and Srinath V. Ekkad. 2017. “Characterization of Heat Transfer Enhancement and Frictional Losses in a Two-Pass Square Duct Featuring Unique Combinations of Rib Turbulators and Cylindrical Dimples.” *International Journal of Heat and Mass Transfer* 106: 629–47. https://www.sciencedirect.com/science/article/pii/S0017931016320634 (February 12, 2018).

Singh, Prashant, Bharath Viswanath Ravi, and Srinath V. Ekkad. 2016. “Experimental and Numerical Study of Heat Transfer due to Developing Flow in a Two-Pass Rib Roughened Square Duct.” *International Journal of Heat and Mass Transfer* 102: 1245–56. https://www.sciencedirect.com/science/article/pii/S0017931016310183 (February 12, 2018).

Stiglich, J J et al. 1998. “The Thermal Inertia Analysis Technique in Gas Turbine Component Reliability Assessment.” *Materials Solutions’98*: 138–44.

Swiderski, W. 2009. “The Characterization of Defects in Multi-Layered Composite Materials by Thermal Tomography Methods.” *Acta Physica Polonica A* 115(4): 800–804.

Urich, Robert H., and Maurice A. Freeman. 1979. “Eddy Current Probe For Inspecting Interiors Of Gas Turbines, Said Probe Having Pivotal Adjustments And A Borescope.”

Vardar, N., and A. Ekerim. 2007. “Failure Analysis of Gas Turbine Blades in a Thermal Power Plant.” *Engineering Failure Analysis* 14(4): 743–49.

Woodmansee, Donald. 2002. “System and Method of Automated Part Evaluation Including Inspection, Disposition Recommendation and Refurbishment Process Determination.” 1(19).

Zorner, Walter. 1995. “Method And Apparatus For Detecting And Locating Defects In A Component Of A Turbine.”

APPENDIX

A.1 Vane position correction for thermal performance characterization

Even with careful mounting of the infrared camera and the test rig, every time a vane was replaced with another, a small spatial displacement was observed as depicted in Figure 25.

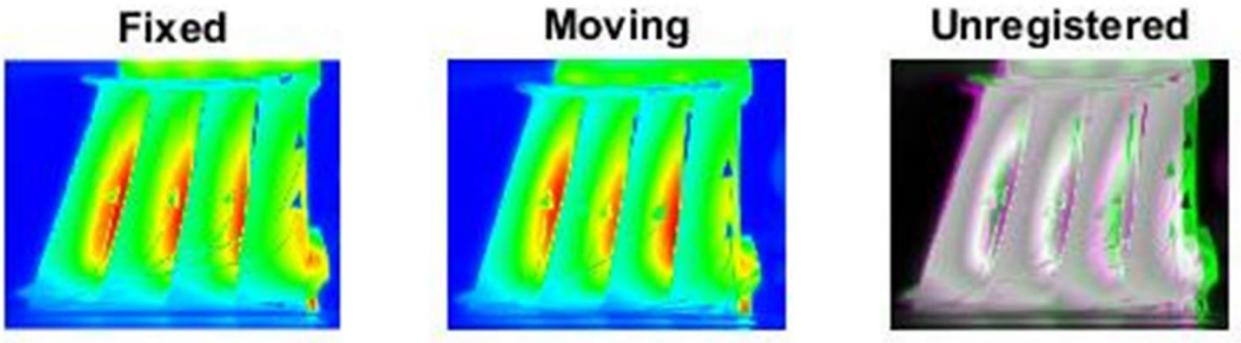

Figure 25: Displacement after vane replacement as seen by the IR camera

Since the technique relies on averaging and comparing pixel level data, it was necessary to make sure correct pixel readings were used. A code was developed in MATLAB that takes as input a video file recorded using the infrared camera and maps the starting frame to a reference image. This is done for all subsequent frames and all datasets corresponding to the various experiments. This procedure made sure that all images and comparisons were based off the same reference. Figure 26 shows the before-and-after correction pictures for a typical vane. Besides, as has been mentioned before, the test rig was quite robust and did not allow for displacement much beyond a couple of millimeters. This was necessary because the relative orientation of the camera and the vane impacts the surface emissivity. As such, even though the code could correct the displacement, too much variation would impact the emissivity resulting in recording incorrect surface temperatures.

In essence, developing the code helped in building a robust methodology for vane-to-vane comparison without the need to purchase precision equipment.

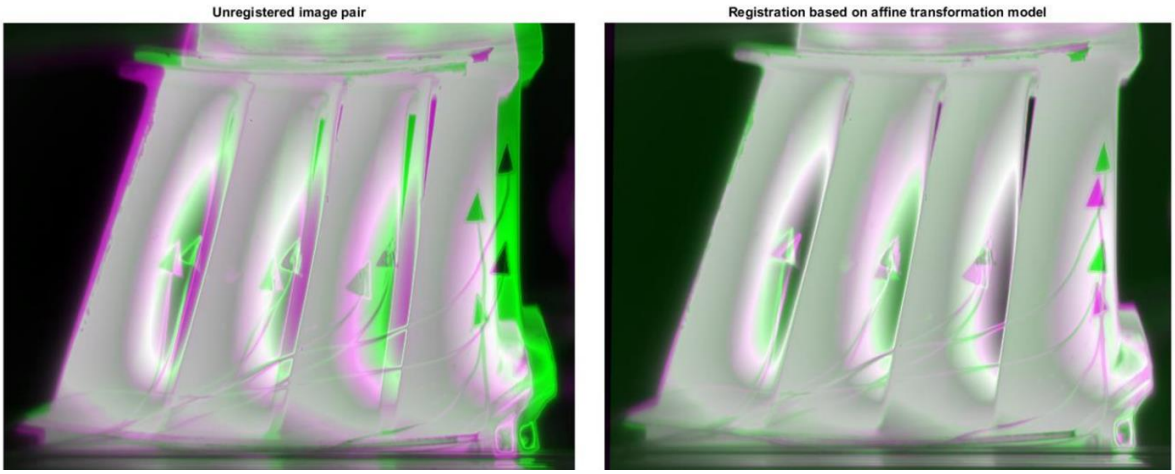

Figure 26: Before and after applying superposition code

A.2 Other Normalizing parameters

Before finalizing on the parameter T*, other normalization parameters were also considered. One such example is described below:

$$\theta = \frac{T_{inlet}(t) - T_{vane}(t)}{T_{inlet(t_0)} - T_{vane(t_0)}}$$

Where: t_0 signifies initial time

t is any time instant t seconds after t_0

The evolution of actual temperature with time for multiple points on the surface of a typical vane is shown in **Error! Reference source not found.** a) while b) shows the variation of the parameter θ. The idea was to find the range of values of the parameter θ, first, for the OEM sample and then compare each repaired part against the observed bound.

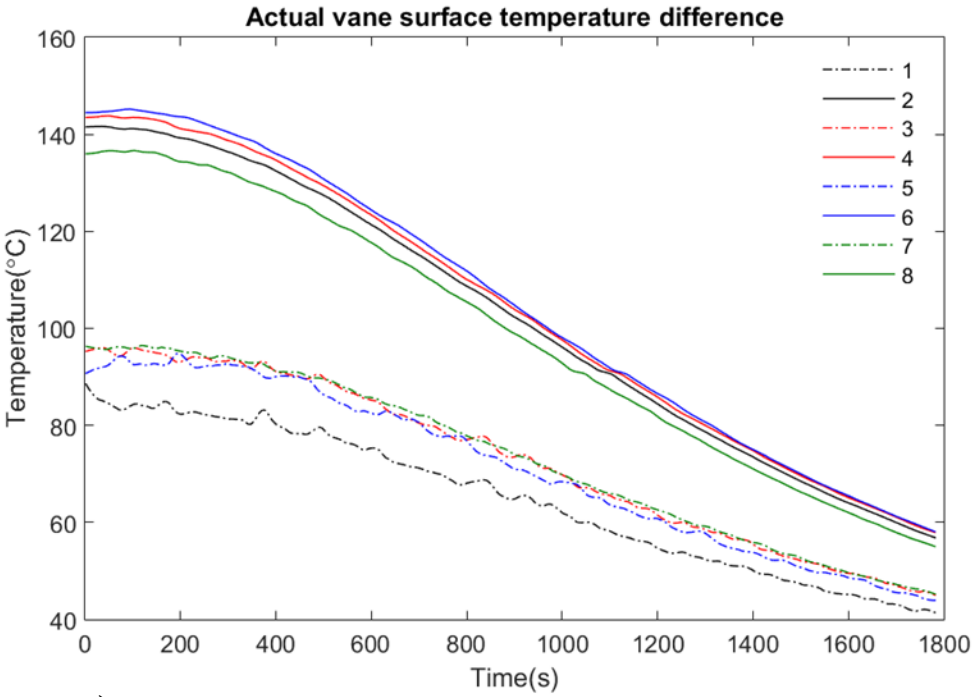

a)

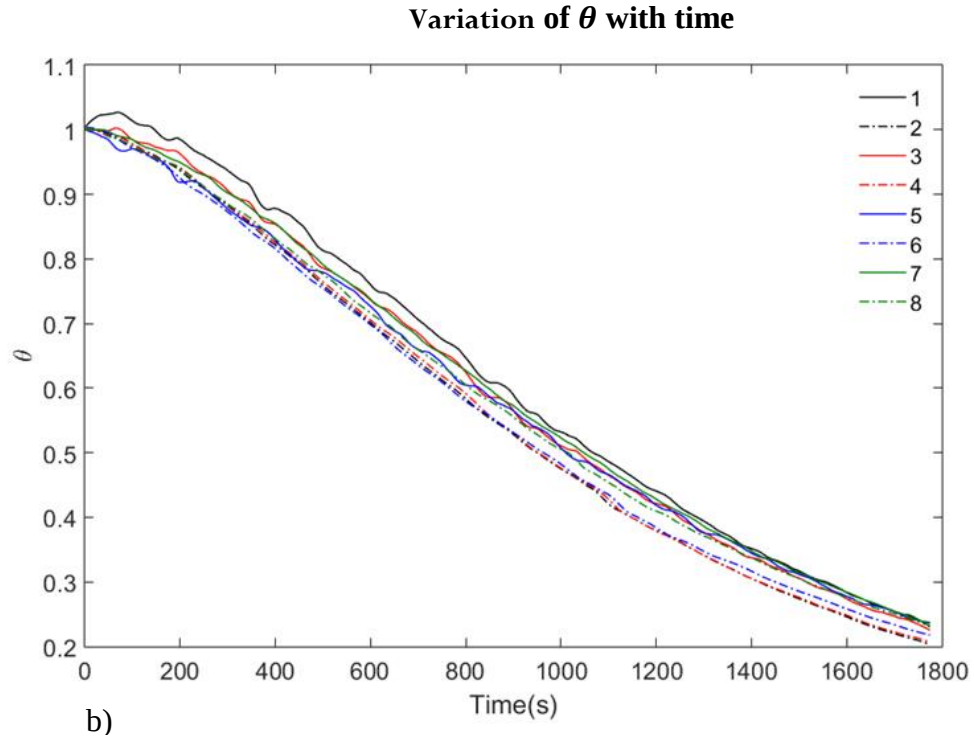

b)

Figure 27: a) Variation of surface temperature for multiple points on a vane as seen by the IR camera; b) Variation of θ for the same points

Bounds created using OEM samples and the variation of θ for a repaired part at the corresponding location is shown in Figure 28. The shaded area is found by comparing the maximum and minimum θ value among all OEM samples at the same location for a particular time instant.

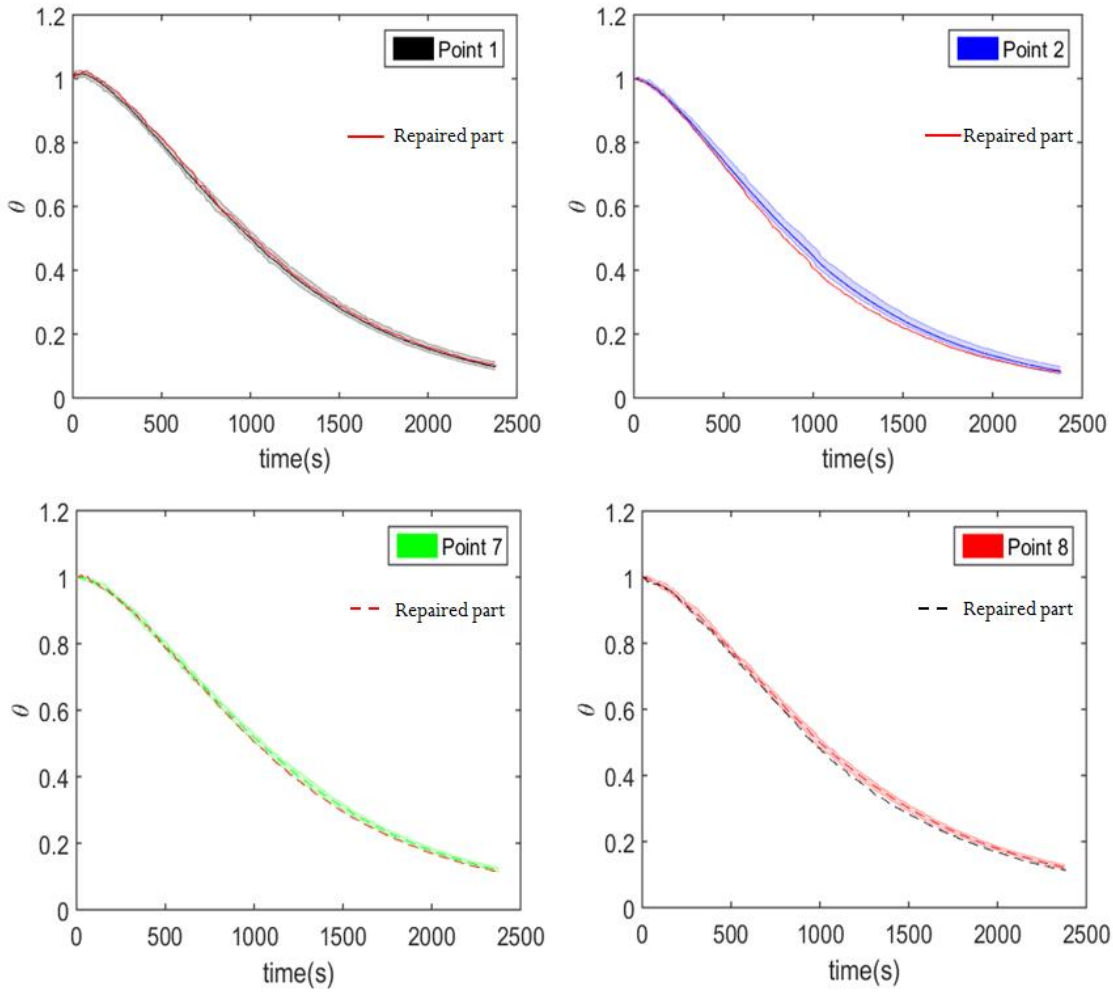

Figure 28: Comparison of θ between multiple points on repaired parts to the bounds of OEM parts.

Conclusions, however, were not straightforward to draw from the data presented above. One particular idea that was explored to gauge the thermal performance was to find the percentage of the vane surface area that was outside of the OEM bounds at any time instant. However, there was an inherent dichotomy is this procedure: say a part is outside the OEM bounds for a major fraction of time but only by a very small amount. Contrast it against another part which is farther outside the bounds but for a shorter duration. Can we say one

passes and the other fails? Perhaps also including the amount of deviation as a factor in the thermal characterization can provide better answers instead of just using a binary switch of ‘inside’ or ‘outside’ bounds. The volume of testing required to determine this was found to be not trivial and was, thus, not pursued further.